CIVIL ENGINEERING STUDIES
Illinois Center for Transportation Series No. 12-014
UILU-ENG-2012-2023
ISSN: 0197-9191

LOAD RATING AND RETROFIT TESTING OF BRIDGE TIMBER PILES SUBJECTED TO ECCENTRIC LOADING

Prepared By
Pablo Caiza
Moochul Shin
Bassem Andrawes
University of Illinois at Urbana-Champaign

Research Report FHWA-ICT-12-014

A report of the findings of
ICT-R27-82
Strengthening of Bridge Wood Pilings Retrofits for Moment Resistance

Illinois Center for Transportation

November 2012

1. Report No.	2. Government Accession No.	3. Recipient's Catalog No.
FHWA-ICT-12-014		

4. Title and Subtitle: Load Rating and Retrofit Testing of Bridge Timber Piles Subjected to Eccentric Loading	5. Report Date November 2012
	6. Performing Organization Code
7. Author(s) Pablo Caiza, Moochul Shin, Bassem Andrawes	8. Performing Organization Report No. ICT-12-014 UILU-ENG-2012-2023
9. Performing Organization Name and Address Illinois Center for Transportation Department of Civil and Environmental Engineering University of Illinois at Urbana-Champaign 205 N. Mathews, MC 250 Urbana, IL 61801	10. Work Unit (TRAIS) 11. Contract or Grant No. R27-82
12. Sponsoring Agency Name and Address Illinois Department of Transportation Bureau of Materials and Physical Research 126 East Ash St. Springfield, IL 62704	13. Type of Report and Period Covered 14. Sponsoring Agency Code

15. Supplementary Notes

16. Abstract

This report first evaluated the load rating procedure currently in use by the Illinois Department of Transportation (IDOT) for rating timber piles supporting multiple-span, simply supported bridges. For simplicity, these piles are often rated under concentric loads, and the effect of bending in the piles is neglected. Recent studies have shown, however, that under highly eccentric live loads, the effect of bending moments in the piles is of great importance and could have an impact on the piles' load rating. The report proposed an alternative structural load rating method for timber piles based on the National Design Specification for Wood Construction (NDS), which took into consideration the effect of combined compression-flexure behavior of piles. This method was used to conduct a parametric study to investigate the effect of several geometric and structural parameters on the load rating of bridge timber piles using 3-D finite element models of concrete deck bridges supported on groups of timber piles. The results showed that the proposed load rating method produced significantly lower ratings for piles with moderate to high levels of deterioration, as compared to the ratings obtained using the conventional approach. Among the studied parameters, the length of piles was found to have the most significant impact on the load rating of the piles. The report also presents a study on examining a fiber reinforced polymer (FRP)-based retrofitting method for timber piles subjected to combined axial and bending loading. A total of twenty pile specimens were tested in the study, four under compression-only load and sixteen under compression-flexure load. Each specimen was tested twice, before and after retrofitting with glass FRP (GFRP) or carbon FRP (CFRP) sheets. To assess the impact of realistic field conditions, different details of the FRP retrofit technique were investigated, including using mortar shell, introducing a mortar-filled wedge in the tested specimen to mimic the effect of decayed wood, and "posting" the piles with nails instead of steel drift pins. The test results showed that the strength of the tested specimens using the proposed GFRP retrofit technique was fully recovered or even enhanced compared to that of the unretrofitted specimens, regardless of the retrofit details adopted in the tests. On average, specimens retrofitted with GFRPs showed strength 10% greater than that of unretrofitted specimens. The behavior of CFRP sheets, however, was less satisfactory due to the small thickness of the CFRP shell used as a result of the high strength of CFRP compared to GFRP. It was also found from the study that using mortar shell along with FRP sheets helped enhance the stiffness of the retrofitted pile. Finally, linear regression analysis was conducted on the test data to develop a formula that could be used for the design of FRP retrofit for bridge timber piles subjected to axial-bending loading.

17. Key Words	18. Distribution Statement
Load Rating; Bridge Timber Piles, Eccentric Load, Fiber Reinforced Polymers, Retrofit	No restrictions. This document is available to the public through the National Technical Information Service, Springfield, Virginia 22161.

19. Security Classif. (of this report)	20. Security Classif. (of this page)	21. No. of Pages	22. Price
Unclassified	Unclassified	47 +appendix	

ACKNOWLEDGEMENT AND DISCLAIMER

This report is based on the results of project no. R27-82 titled “Strengthening of Bridge Wood Pilings Retrofits for Moment Resistance.” R27-82 was conducted in cooperation with the University of Illinois at Urbana-Champaign and the Illinois Department of Transportation. The authors would like to thank undergraduate students You Li and A. El Kharbotly, as well as lab staff members, T. Prunkard and D. Marrow of the University of Illinois at Urbana-Champaign for their contributions to the execution of the experiments. Special thanks to the members of the IDOT Technical Review Panel (TRP) for their invaluable ideas and suggestions throughout this research. The contents of this report reflect the view of the authors, who are responsible for the facts and the accuracy of the data presented herein. The contents do not necessarily reflect the official views or policies of the Illinois Department of Transportation. This report does not constitute a standard, specification, or regulation.

EXECUTIVE SUMMARY

This report first evaluated the load rating procedure currently in use by the Illinois Department of Transportation (IDOT) for rating timber piles supporting multiple-span, simply supported bridges. For simplicity, these piles are often rated under concentric loads, and the effect of bending in the piles is neglected. Recent studies have shown, however, that under highly eccentric live loads, the effect of bending moments in the piles is of great importance and could have an impact on the piles load rating. The report proposed an alternative structural load rating method for timber piles based on the National Design Specification for Wood Construction (NDS; AFPA 2005), which took into consideration the effect of combined compression-flexure behavior of piles. This method was used to conduct a parametric study to investigate the effect of several geometric and structural parameters on the load rating of bridge timber piles using 3-D finite element models of concrete deck bridges supported on groups of timber piles. The results showed that the proposed load rating method produced significantly lower ratings for piles with moderate to high levels of deterioration, as compared to the ratings obtained using the conventional approach. Among the studied parameters, the length of piles was found to have the most significant impact on the load rating of the piles.

The report also presented a study on examining fiber reinforced polymer (FRP)-based retrofitting method for timber piles subjected to combined axial and bending loading. A total of twenty pile specimens were tested in the study, four under compression-only load and sixteen under compression-flexure load. Each specimen was tested twice, before and after retrofitting with glass FRP (GFRP) or carbon FRP (CFRP) sheets. To assess the impact of realistic field conditions, different details of the FRP retrofit technique were investigated, including using mortar shell, introducing a mortar-filled wedge in the tested specimen to mimic the effect of decayed wood, and "posting" the piles with nails instead of steel drift pins. The test results showed that the strength of the tested specimens using the proposed GFRP retrofit technique was fully recovered or even enhanced compared to that of the unretrofitted specimens, regardless of the retrofit details adopted in the tests. On average, specimens retrofitted with GFRPs showed strength 10% greater than that of unretrofitted specimens. The behavior of CFRP sheets, however, was less satisfactory due to the small thickness of the CFRP shell used as a result of the high strength of CFRP compared to GFRP. It was also found from the study that using mortar shell along with FRP sheets helped enhance the stiffness of the retrofitted pile. Finally, linear regression analysis was conducted on the test data to develop a formula that could be used for the design of FRP retrofit for bridge timber piles subjected to axial-bending loading.

TABLE OF CONTENTS

LIST OF FIGURES

LIST OF TABLES

CHAPTER 1 INTRODUCTION

The relatively limited maintenance and attention that small rural bridges often receive throughout their service life could potentially result in the rapid deterioration of these bridges' structural conditions. Consequently, and along with the current consistent increases in loading demands, some of these bridges may reach a point where they fail to accommodate traffic volumes, vehicle sizes, and weights. A clear example of this problem is Bridge No. 019-5010 in DeKalb County, Illinois, which collapsed on August 19, 2008.

The bridge consisted of three 42-feet spans skewed 45°. The superstructure comprised prestressed concrete deck beams simply supported on concrete pile caps and timber piles. The bridge was constructed in 1976 according to American Association of State Highway Officials (AASHTO) HS-20 load criteria. One of the mid-span bents failed and, as a result, two spans of the bridge collapsed (Figure 1-1a). The collapsed bent had eight piles and additional diagonal cross bracings (Figure 1-1b). It is important to note that the top 6 feet of two of the piles were removed and replaced in the year 2000 during maintenance work, yet these two piles were completely uprooted during the bridge collapse. Figure 1-1c shows the position of these uprooted piles. A forensic study (Borello et al. 2009) indicated that the current load rating method, which takes only the concentric load into account, can lead to the over-rating of the capacity of timber piles. Most important, the study concluded that the effect of eccentrically applied loads should be considered when determining the capacity of bridges supported on timber piles.

Furthermore, because the replacement of bridges supported on deteriorated timber piles is expensive, every effort is needed to develop sound and cost-effective retrofit measures that can effectively extend the service life of these structures. The collapse of the DeKalb County bridge also sheds light on the limitation of currently used retrofit techniques in restoring the flexural capacity of deteriorated piles.

Therefore, this report focuses on (1) developing a new load rating method for bridge timber piles under eccentric loading and (2) developing a simple and reliable retrofit technique using fiber reinforced polymers (FRPs) to enhance the flexural-compression behavior of aged and deteriorated timber piles.

(a) (b)

(c)

Figure 1-1. Collapse of Bridge No. 019-5010 DeKalb County, Illinois, 8-19-2008: (a) mid-span bent after collapse, (b) remaining mid-span bent (identical to the one that failed), (c) position of uprooted piles.

The current code provisions for the load rating of bridge timber piles follow the allowable stress design (ASD) method. This takes into consideration, as explained above, only the concentric compressive loading on piles, assuming that the superstructure has sufficient rigidity to prevent the effect of eccentricity on the piles, in accordance with the LRFD Bridge Design Specification (AASHTO 2007).

However, if the superstructure has multiple simply supported spans as shown in Figure 1-2a, the increased load on a single span, due to the presence of a vehicular live load, results in different reactions from the adjacent spans. This causes an eccentric compressive force to be transmitted to the piles as shown in Figure 1-2b. The effect of the eccentrically applied force becomes more critical to the integrity of the timber piles, especially deteriorated ones because it increases the demands on these piles to a level that may exceed the level of demands that these piles were designed to withstand.

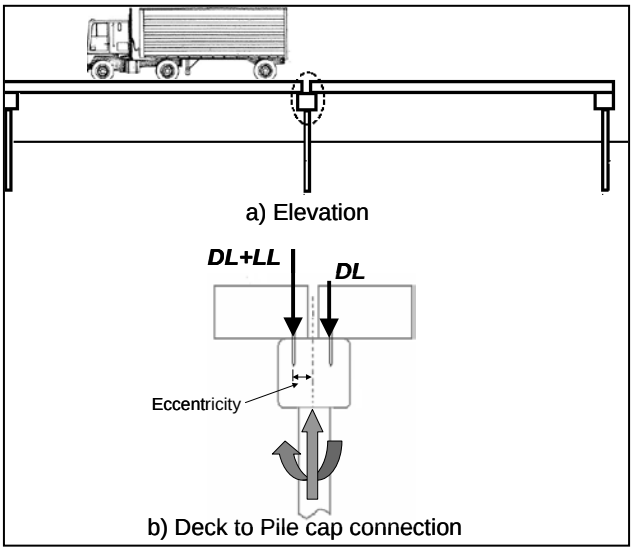

Figure 1-2. Multiple-span, simply supported bridge on timber piles under eccentric loading.

1.1 BACKGROUND

Early investigation into the interaction of combined flexure and compression involved the experimental testing of 2 in. (51 mm) square specimens and analysis based on Euler buckling (Newlin and Trayer 1956). It was found that the material capacity is a function of load eccentricity as well as the slenderness of the section. In a separate study, interaction equations were developed to describe the results from flexure-compression tests as a function of the axial stress and the flexural stress (Wood 1950). The equations showed reasonable accuracy for short, intermediate, and long columns. The results of Buchanan (1986) showed that the linear interaction model between flexure and compression is conservative and suggested non-linear models for inelastic bending. The study also explored the effect of size on the interaction, with small compressive force and large moments. Subsequently, interaction equations were derived to include second-order effects coupling the axial force and bending moment (Zahn 1988). These equations reasonably captured experimental results and were adopted by the current National Design Specification for Wood Construction (NDS; AFPA 2005). A recent study fitted the existing design models for flexure-compression interaction to interaction tests conducted on rectangular solid-spruce specimens (Steiger and Fontana 2005). Non-linearity of the interaction was discussed based on the elastic stress-strain relationship in the tension portion and the non-linear, “plastic” behavior of the compression zone.

Experimental tests, such as those conducted to investigate the collapse of the bridge in DeKalb County, showed a 60% reduction in the capacity of eccentrically loaded piles compared to that of concentrically loaded specimens (Borello et al. 2009, 2010).

Even though previous studies have explored the interaction of flexure and compression in wood specimens, procedures to obtain the capacity of timber specimens

subjected to flexure and compression and their use in evaluating pile load ratings of bridges with timber pile foundations still remain to be developed.

Another main aspect of this report focuses on retrofitting timber piles. Clearly, bridges supported on timber piles are vulnerable to extreme loadings as well as harsh environmental conditions that, if not monitored regularly, could lead to the rapid decay of the wood (McCutcheon et al. 1986). In the United States and other parts of the world, measures are often taken to delay or prevent the decay of bridge timber piles, such as the use of creosote oil and regular inspection of the piles. If inspection reveals that a portion of the pile is in a bad condition and in need of replacement, a common technique known as "posting" is utilized. "Posting" a pile is a process in which a portion of the pile is cut out and replaced with a new piece of timber (Figure 1-3). This new piece is connected to the existing pile by embedded metal fasteners (Wipf et al. 2003). The two piles removed and replaced in the failed DeKalb County bridge used this technique. The post connection at the interface between the existing timber and the new timber is capable of transmitting axial compression forces, but it is not designed to transfer moment. Nonetheless, due to its cost-effectiveness, this type of retrofit technique is generally preferred over a complete replacement of the entire pile or encasing the timber pile in a thick, reinforced concrete shell.

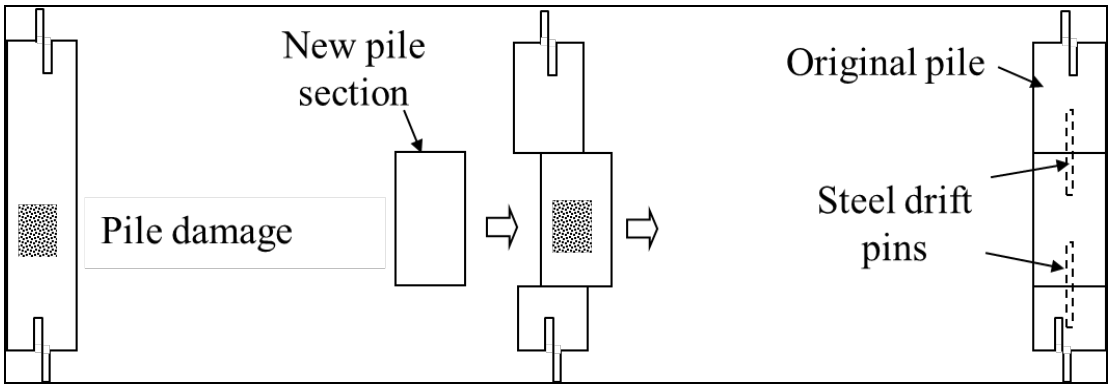

Figure 1-3. Replacement of a wood piece from a damaged timber pile.

Although the pile "posting" retrofit technique is commonly used, its limited ability to restore the flexural capacity of the piles is considered a major drawback that could potentially cause severe consequences, as in the case of the failed Dekalb County bridge.

One of the relatively recent approaches studied to restore the original load-carrying capacity of heavily decayed timber piles is the use of FRP wraps on the top of a relatively thin cementitious grout shell around the timber pile. In most of the research done in this area, glass FRP (GFRP) wraps are used to confine the grout shell and the timber core in such a way that only the axial compression capacity of the piles is improved (Hagos 2001). No studies, to the knowledge of the authors, have been conducted specifically to investigate the combined flexure-compression behavior of timber pile post connections retrofitted with FRPs.

CHAPTER 2 LOAD RATING PROCEDURE

An existing load rating method, which takes only concentric load into account, can overestimate the capacity of a timber pile. However, a timber pile is often subjected to an eccentric load, which is critical to the capacity of the timber pile. Therefore, in this chapter, a new load rating method (Andrawes and Caiza 2012) is discussed and developed.

2.1 CURRENT PRACTICE

The allowable stress design (ASD) method is currently used in rating bridge timber piles. For the purpose of simplicity, the piles are rated under concentric axial loads and the effect of bending is neglected. For example, the load rating of timber piles under concentric axial loads using the HS20-44 truck is defined as follows:

$$\text{Pile Rating} = \frac{\text{[Pile Capacity - Dead Load]}}{\text{HS20-44 Live Load}} \text{ X } 20 \qquad (2.1)$$

The load rating is obtained in two steps: (1) calculation of the axial loads on the pile due to dead load and live load, and (2) evaluation of the capacity of the timber pile, which is representative of the maximum allowable compressive force in the pile. The axial loads in each of the piles are typically calculated by performing a simple frame analysis of the pile cap and timber pile system. The reaction of the deck on the pile cap is calculated, and the simplified frame is subjected to an equivalent uniformly distributed load. The capacity of the timber pile is twofold: when the pile driving data is available, the "as-driven" pile resistance may be used to limit the pile capacity to an expected geotechnical capacity. Existing piles inherently provide a time-tested demonstration of their geotechnical capacity. Nearly all timber piling jobs use the Engineering News Formula for their driving capacity, which calculates the design capacity based on the weight of the driving hammer, height of drop, and the final set of the pile (Chellis 1967).

The pile driving capacity varies among state departments of transportation (DOTs). For example, the Illinois DOT uses 51 kips (226.86 kN) as the upper geotechnical boundary condition to which a timber pile could have been driven based on past policies, while the Iowa DOT uses a capacity limit of 69 kips (308.57 kN) for piles of length 20 ft (6.1 m) to 35 ft (10.67 m) and with a minimum tip diameter of 8 in. (20.32 cm) (Iowa DOT 2010). The structural capacity of the timber pile, on the other hand, is determined using the NDS formula shown in Equation 2.2 for the allowable compressive stress parallel to grain, F_c' (AFPA 2005).

$$F_c' = F_c \times C_D \times C_t \times C_u \times C_p \times C_{cs} \times C_{sp} \qquad (2.2)$$

In Equation 2.2, F_c is the reference compression design value for treated round timber piles, which varies depending on the species of timber. In this study, the value of

F_c is taken as 1.10 ksi (7.584 MPa), which corresponds to red oak. This value is multiplied by pertinent adjustment factors to obtain F_{cDL}' and F_{cLL}', the allowable compressive stress due to dead load and live load, respectively. Table 2-1 lists the adjustment factors used in Equation 2.2, their significance, and the values used for calculations per the NDS (AFPA 2005) recommendations.

Table 2-1. Adjustment Factors for Allowable Compressive Stress

Adjustment Factor	**Significance and Values Used**
C_D	*Load Duration Factor* C_D = 0.9 (permanent duration) for calculation of allowable compressive stress under dead load (F_{CDL}') C_D = 1.15 (2-month duration) for calculation of allowable compressive stress under live load (F_{CLL}')
C_t	*Temperature Factor* C_t = 1 for temperatures below 38°C
C_u	*Untreated Factor* C_u = 1 for treated piles
C_p	*Column Stability Factor* Calculated using F_{cE} and c from Equation 2.3
C_{cs}	*Critical Section Factor* Depends on the location of the critical section C_{cs} = 1 is assumed
C_{sp}	*Single Pile Factor* Depends on load sharing patterns in a pile cluster C_{sp} = 1 is assumed

The column stability factor C_p, calculated by the Ylinen formula, represents the interaction of the buckling and crushing modes of failure (Zahn 1988).

$$C_p = \frac{1+\left(F_{cE}/F_c^*\right)}{2c} - \left[\left(\frac{1+\left(F_{cE}/F_c^*\right)}{2c}\right)^2 - \frac{F_{cE}/F_c^*}{c}\right]^{1/2} \qquad (2.3)$$

where $F_c^* = F_c * C_D * C_t * C_u * C_{cs} * C_{sp}$. The Euler critical buckling stress (F_{cE}) is calculated using the following equation.

$$F_{cE} = \frac{0.822 E_{\min}'}{\left(l_e / d\right)^2} \tag{2.4}$$

where $E_{\min}' = E_{\min}$ (reference modulus of elasticity) $\times C_t$. The effective length l_e is taken as the exposed pile length (above the soil or mud line) in addition to an embedment length until theoretical fixity is reached. A constant embedment length of 3 ft. (914.4 mm) is typically used. In case of damaged piles, the dimension of the face of an equivalent square column, *d* is calculated for the undamaged area of the pile. The value *c* for round timber piles is taken as 0.85 (AFPA 2005).

This current load rating method takes into consideration only the axial compressive force in the pile. The effect of the interaction of the axial forces and flexure in the pile on the pile capacity is completely neglected.

2.2 PROPOSED MODIFICATION

Further analysis of Equation 2.1 reveals that the difference between the pile capacity and dead load in the numerator can be interpreted as the concentric structural live load capacity. This is compared to the denominator, which represents the live load in the pile due to the HS20-44 loading. The proposed modified load rating equation is shown below.

$$\text{Structural Pile Rating} = \left(\frac{\text{LL Stress Capacity, } f_{cLL}\big|_{\max}}{\text{Stress due to HS20-44 Live Load}} \right) \times 20 \tag{2.5}$$

Because the stress distribution on a pile section is non-uniform under eccentric load, the modified load rating equation used in this study (Equation 2.5) compares the centroidal live load stress capacity, $f_{cLL}\big|_{\max}$ in the pile to the centroidal stress induced under the rating vehicle, which in this study was taken as the HS20-44 truck to obtain the structural load rating. Instead of using Equation 2.2 to calculate the LL stress capacity, the alternative load rating method suggests using the interaction equation (Equation 2.6), presented in the NDS (2005) for wood members subjected to axial compression and bending. Note that the eccentricity due to dead load is ignored in this inequality.

$$\left(\frac{f_{cDL}}{F_{CDL}'} + \frac{f_{cLL}}{F_{CLL}'} \right)^2 + \frac{f_{cLL}\left(\frac{6e_{LL}}{d} \right) \times \left[1 + .234 \frac{f_{cLL}}{F_{cE}} \right]}{F_b' \left(1 - \left(f_{cLL} / F_{cE} \right) \right)} \le 1.0 \tag{2.6}$$

This inequality is applied for a single pile where:

f_{cDL} (dead load centroidal stress) = Dead Load Reaction / Effective Area

f_{cLL} = centroidal stress due to live load only (to be determined from the inequality)

F_{CDL}', F_{CLL}' = allowable compressive stress parallel to grain due to dead load and live load, respectively (from Equation 2.2)

F_{cE} = Euler critical buckling stress (from Equation 2.4)

$F_b' = F_b$ (reference design bending value for timber species) $\times C_D \times C_t \times C_u \times C_p \times C_{cs} \times C_{sp}$

e_{LL} = eccentricity at which live load is applied

The value of eccentricity at which live load is applied, e_{LL}, is conservatively taken as 60% of the physical eccentricity of the deck with respect to the pile cap. This percentage was obtained by examining the moment developed in the timber pile group as the eccentricity of the deck was varied across a range of values using finite element models.

$$e_{LL} = 0.6 \times physical\ eccentricity\ of\ the\ deck \tag{2.7}$$

For a single pile under the effect of dead load stress, f_{cDL}, and live load eccentricity, e_{LL}, the maximum LL capacity under eccentric loading, $f_{cLL}\big|_{\max}$, is determined by solving the left-hand side of Equation 2.6 for 1.0. This is subsequently used in Equation 2.5 to obtain the modified structural pile rating. The lower of the structural rating described in this section and the load rating based on the expected geotechnical capacity governs the load rating of the timber pile in the field. It is worth noting that the stresses due to dead loads and HS20-44 live loads can be obtained by performing a simple frame analysis or by conducting a more detailed finite element (FE) analysis.

CHAPTER 3 PARAMETRIC STUDY

To understand the effect of the different bridge geometric characteristics on the modified structural load rating, a series of bridge models were developed and analyzed. Detailed finite element (FE) models were utilized to account for the possible effect of certain geometric parameters of the bridge, such as the skew angle and eccentricity of the deck on the pile cap on the load rating of the pile. Also, the critical position of the vehicular lane load on the bridge span was considered to study the effect of the variation of a number of geometric parameters on the modified structural load rating. The geometric parameters of the FE model were varied over a practical range of values to study the effect of their variation on the modified structural load rating. Three common deterioration profiles observed in piles were also used in these models to obtain their rating at different levels of deterioration.

3.1 BRIDGE PARAMETERS

The proposed rating procedure, along with the FE method, was employed in this project to study the impact of five structural and geometric parameters, including span length, eccentricity of the deck, length of pile above the soil, skew angle, and level of deterioration of the piles, on the rating of bridge timber piles. A constant embedment length of 15 ft (4.57 m) below the soil was assumed for all piles. A practical range for each of these parameters was obtained from studying the design plans of an inventory of multiple-span bridges supported on timber piles in Illinois. The ranges of these parameters are shown in Table 3-1, along with the average values selected for each parameter to be used in the prototype bridge model, as will be discussed later.

Table 3-1. Range and Average Values of Geometric Structural Parameters

Parameter	Range	Prototype Bridge Value
Span Length, ft (m)	19.9 – 42.6 (6.07 – 13.00)	30.7 (9.36)
Eccentricity of the Deck, in. (mm)	4.0 – 7.5 (102 – 191)	5.7 (146)
Total Length of Pile, ft (m)	24 – 32 (7.32 – 9.75)	28 (8.53)
Skew Angle	0° – 45°	25°

The study of the design plans of these simply supported bridges revealed that the number of piles per abutment or pier varied between six and eight. These piles were typically embedded up to 15 ft (4.57 m) into the soil. Common species of timber used for piles in these bridges are Red Oak, Douglas Fir, and Southern Pine. Two common types of concrete bridge decks were observed: precast, not prestressed, reinforced beam/slab

system and voided precast, prestressed concrete beams. In some plans, a system comprising beams parallel and perpendicular to the longitudinal axis of the bridge was used. Precast and prestressed beams were used in many cases. The number of spans varied from two to three.

3.2 DETERIORATION OF TIMBER PILES

The decay of aged timber piles imposes significant risk on the strength of bridges supported by these pile types. The level of deterioration significantly impacts the values of allowable compressive stresses, F'_{cDL} and F'_{cLL}. For the purpose of this study, three distinct profiles of pile deterioration are explored. These distinctive deterioration profiles have been selected based on a review of typical types of pile deterioration observed in the field. The deterioration profiles are shown in Figure 3-1.

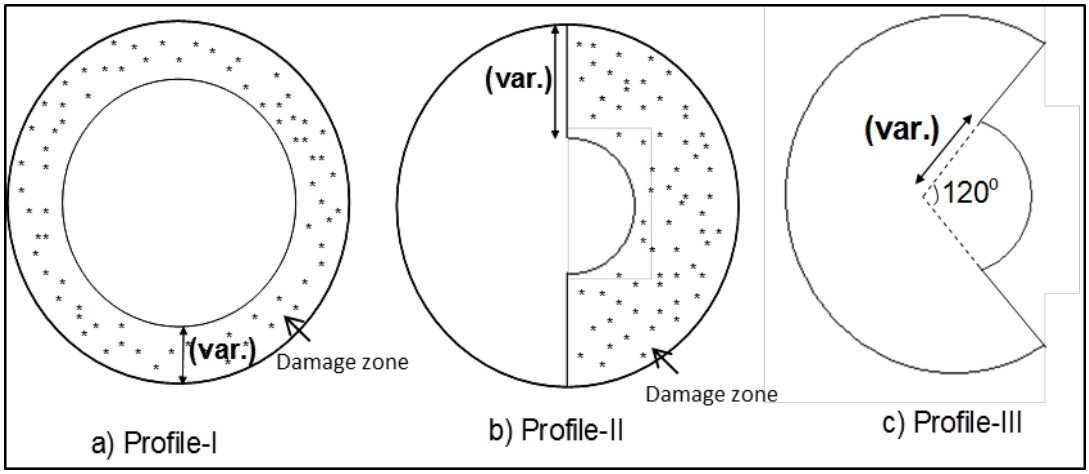

Figure 3-1. Deterioration profiles considered in the analysis.

Each deterioration profile is assigned varying levels of damage. Based on field observations (Borello et al. 2009), it was assumed that the deterioration exists only above the mud line. The level of damage in each deterioration profile is increased until the structural rating of the pile falls below the expected geotechnical capacity and governs, for each of the four parameters considered in the study.

The first deteriorated section (Figure 3-1a) involves concentric damage around a uniform periphery of the timber pile. The width of the periphery is varied to obtain varying levels of deterioration. The second section (Figure 3-1b) shows eccentric damage, with half of the pile still capable of sustaining the load and an undamaged semicircular core; the remaining portion is deteriorated. The radius of the semicircular core is varied to obtain variable deterioration levels. The third section (Figure 3-1c) depicts a portion of the pile that has completely worn away due to decay. The pile has an outer periphery that is non-existent through a 120° angle and has an inner core of a certain radius. The radius of the inner core and the angle of the sector are varied to obtain

different deterioration levels. To obtain the critical case of loading, the section is placed such that the eccentric vehicular live load acts on the damaged portion of the pile.

3.3 PROTOTYPE BRIDGE

A two-span bridge with precast concrete deck beams simply supported by concrete pile caps was used as a prototype in this study. Figure 3-2 shows the layout of the bridge with the values of the average geometrical parameters specified in Table 3-1.

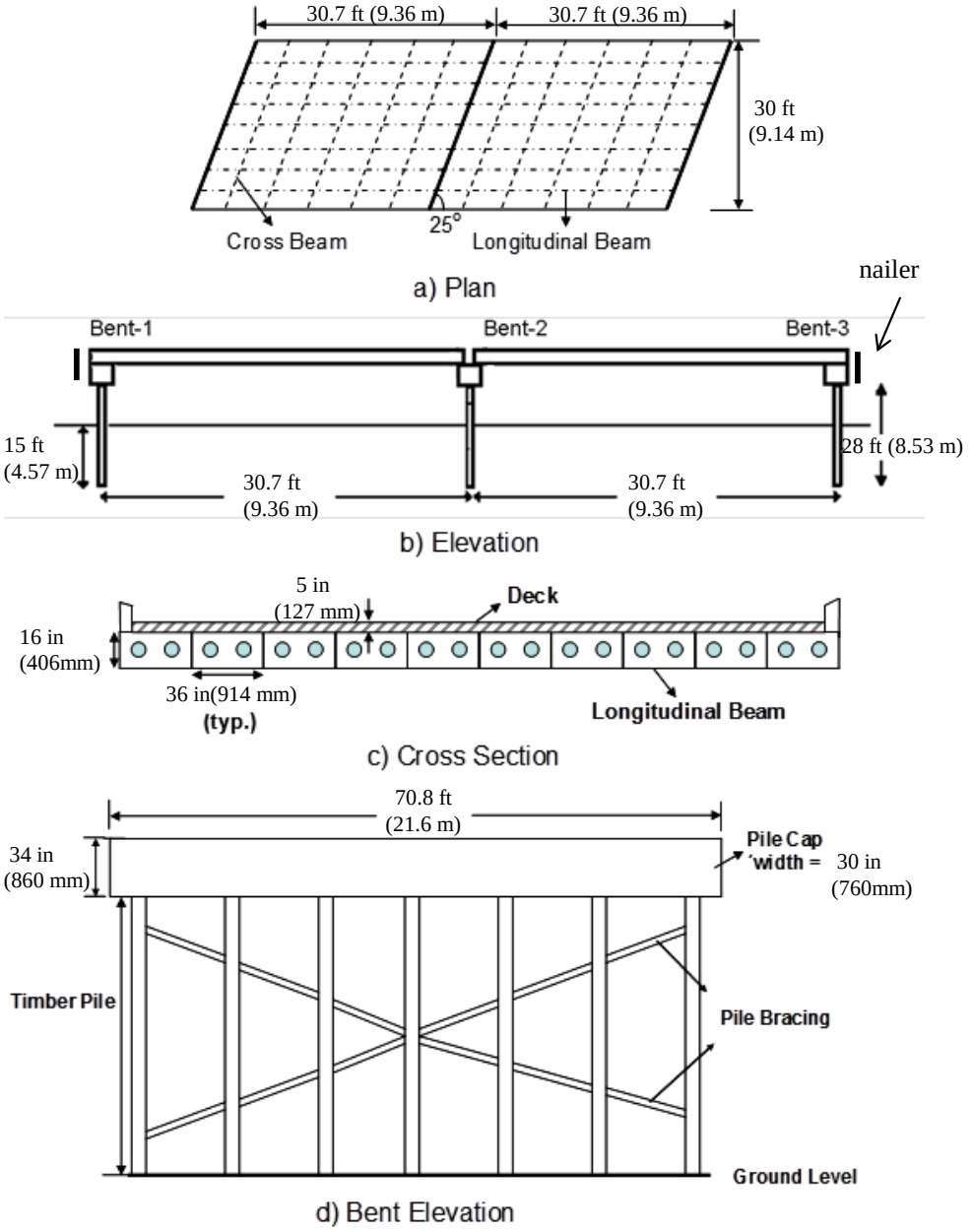

Figure 3-2. Layout of the prototype bridge.

The superstructure comprised a system of precast cross beams and longitudinal beams, approximately 17 in (432 mm) deep, supporting a concrete deck with a thickness of 5 in. (127 mm) (Figure 3-2c). The pile cap is supported by a timber foundation system comprising seven red oak piles of circular cross section with a diameter of 12 in. (305 mm). These piles extend 15 ft (4.57 m) below the river bed. The piles are also braced with rectangular wood members of cross section 3 in. × 12 in. (76 mm × 305 mm) as shown in Figure 3-2d. The ends of pile cap bents 1 and 3 are constrained by wood "nailers" to prevent the movement of the pile caps in the longitudinal direction. The beams supporting the deck are placed at an eccentric distance with respect to the pile cap, as illustrated in Figure 1-2b.

The beams supporting the deck are connected to the pile cap by dowel bars, cast in the pile cap, and inserted into the beam, which releases the rotation of the beam and deck unit with respect to the pile cap about the skewed axis shown in Figure 3-2a. The live load due to vehicular loading on a single span, as shown in Figure 1-2, results in a moment to be transferred to the piles, which are embedded into the rigid pile cap, leading to compression-flexure behavior of the timber piles.

3.4 FE MODEL DESCRIPTION

This section describes the FE model, developed using ANSYS (ANSYS 2004), for the prototype bridge. As explained earlier, the structural parameters of this prototype model were varied to generate further FE models used in the parametric study. The elements and components of the model are shown in Figure 3-3.

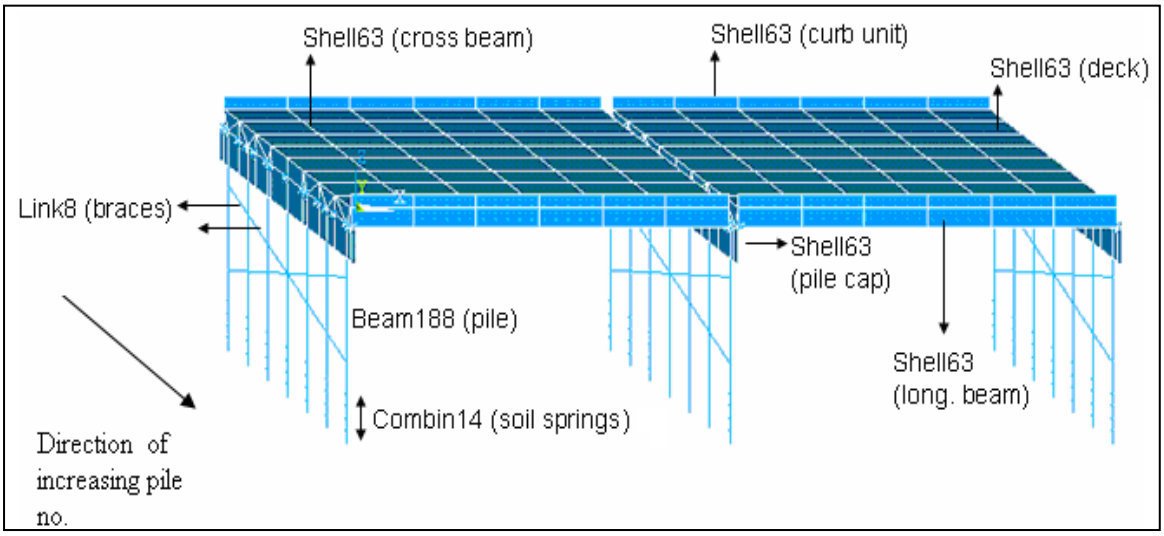

Figure 3-3. Finite element (FE) model of the bridge used in the analysis.

3.4.1 Superstructure

The superstructure of the prototype bridge comprised a system of precast longitudinal and cross concrete beams supporting the deck. These components were modeled using a shell element, SHELL63. The bending moment of inertia of each beam was used to obtain an equivalent thickness for the shell element. Linear elastic behavior of concrete with a modulus of 3800 ksi (26200 MPa) was used.

3.4.2 Pile Caps

The concrete pile caps at the piers and abutments are also modeled using SHELL63. The nodes of the elements used to mesh the pile caps at Bent-1 and Bent-3 (Figure 3-2) are constrained in the longitudinal direction to represent the restraint of the wood "nailers" at the abutments. The eccentric connection shown in Figure 1-2b, between the pile cap and the beam-deck system, has two structural features: (1) it transfers the moment from the beam-deck system to the pile cap and to the piles, and (2) the dowel bars that connect the beam-deck system to the pile cap offer negligible rotational restraint of the deck with respect to the pile cap.

To capture the effect of the moment transfer, a rigid shell element is used to connect the shell elements representing the beam-deck system to the pile cap as shown in Figure 3-4. To model the second feature, the nodes of the rigid shell at the interface of the deck and shell are connected by means of contact pair elements (CONTA175). CONTA175 is used to represent the nature of contact between two distinct nodes by defining the relationship between the degrees of freedom at the two nodes (ANSYS 2004). The nodes on the deck and on the rigid shell are assigned the same displacements for all degrees of freedom except for the rotation about the skewed y-axis. This accurately simulates the nature of this connection.

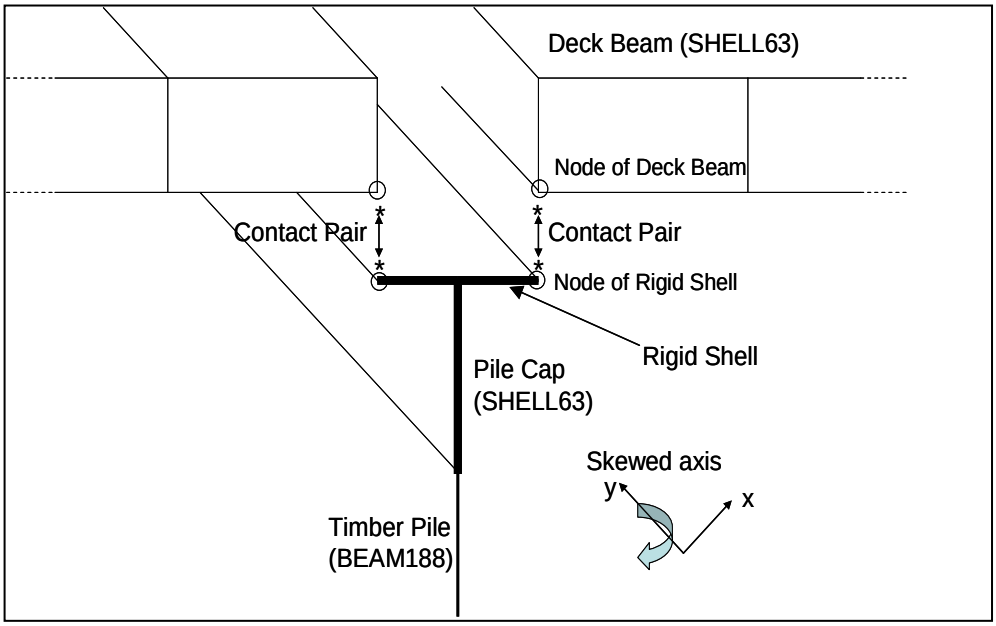

Figure 3-4. Modeling technique of the deck to pile cap connection.

3.4.3 Piles and Pile Braces

The timber pile comprised two portions, 13 ft (3.96 m) length above the soil and 15 ft (4.57 m) embedment into the soil. Preliminary results showed that for the type of soil considered and the level of axial load in the piles, the pile reaches fixity at approximately 5 ft (1.52 m) below the mud line. Therefore, for the purpose of FE modeling, an embedment of 5 ft (1.52 m) below the mud-line, ending in a pin support with translational restraints, was utilized. The timber piles were modeled using 3-D beam element (BEAM188) with a length of 6 in. (152 mm). The element is capable of undergoing large deformations and capturing geometrical and material non-linearity (ANSYS 2004). The fiber section technique is used to define the cross section of the pile. Using FiberSIM-ANSYS, for the undamaged pile, the cross section is divided into fibers in the radial and circumferential directions as shown in Figure 3-5a.

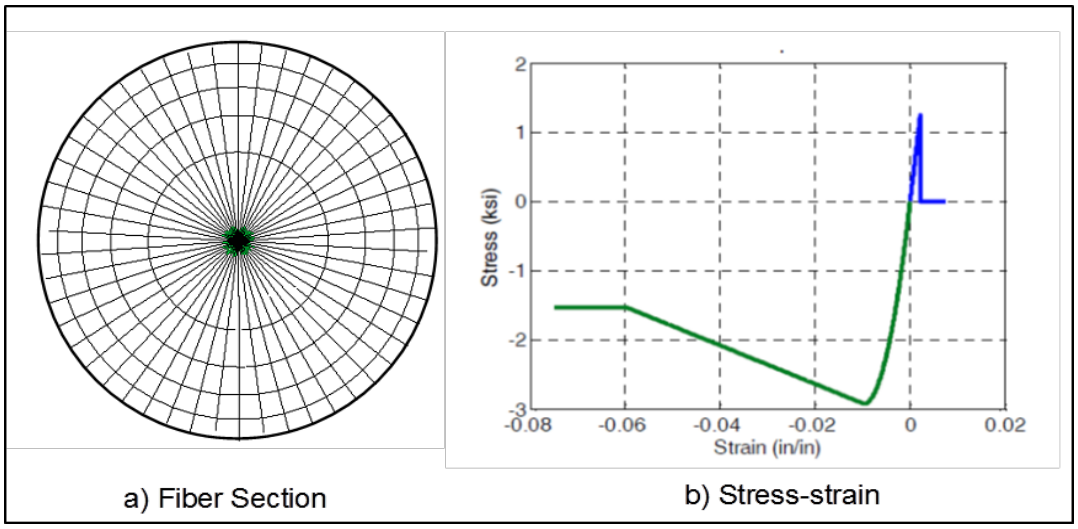

Figure 3-5. (a) Fiber section of the undamaged pile, and (b) stress-strain relationship used to describe the constitutive behavior of the wood.

The non-linear material behavior of wood was assigned to each fiber. This was done using the cast-iron plasticity model (ANSYS 2004), which simulates the uniaxial non-linear constitutive relationship up to the peak compressive strain and peak rupture strain in tension as illustrated in Figure 3-5b. The input parameters required to define this model include an initial modulus of elasticity and the stress-strain data. The input data was obtained from the results of a previous experimental study conducted on real timber piles retrieved from a collapsed bridge in Illinois (Borello et al. 2009).

The cross-sections of the deteriorated piles shown in Figure 3-1 are discretized into fiber sections as shown in Figure 3-6. The deteriorated sections are assigned to those elements which correspond to the pile with the critical/lowest structural rating in the undamaged pile analyses. The damaged area is incapable of sustaining load and the corresponding fiber cells in this region are assumed to have negligible stiffness.

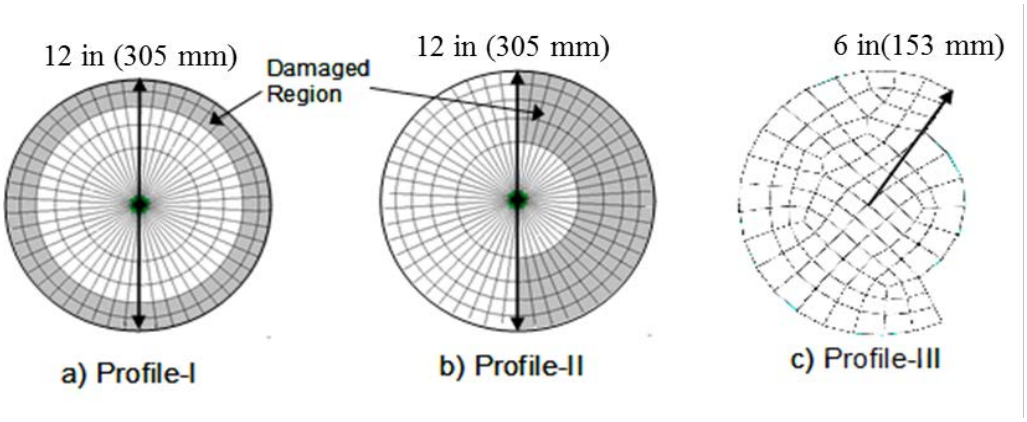

Figure 3-6. Fiber sections used in the FE analysis of the three deterioration profiles.

The pile braces are meshed using the LINK8 element, which is a uniaxial 3-D spar element with three translational degrees of freedom at each node. Because the pile braces are pin-jointed to the timber piles, the bending of these members can be ignored.

3.4.4 Soil-Structure Interaction

The characteristics of the soil-structure interaction used in this study were adopted from a previous study by the first author and others (Borello et al. 2009). The study included in-situ field tests such as the field vane shear test (FVST) and portable dynamic cone penetration test (DCPT). The site considered in the study consisted of stiff to very stiff, low plasticity, glacially overridden loams with variable gravel and cobble content. The field test results were used to model the lateral soil springs that were used to represent the effect of soil in the bridge model. A series of p-y curves was generated for the springs using the program LPile Plus. The multi-linear curves generated by LPile were simplified into tri-linear forms and used in the FE model of the bridge. Preliminary results (Borello et al. 2010) showed that for the type of soil considered, the vertical pile movement due to pile toe resistance is negligible and the use of vertical springs to represent the skin friction has almost no impact on the pile behavior within the considered 5 ft (1.52 m) of embedded pile length until fixity is reached. Therefore, a pin support was used at the end of the 5 ft (1.52 m) embedded length in addition to COMBIN14 elements, which were used only to represent the lateral resistance of the soil in two horizontal and perpendicular directions. The springs were attached to the nodes of the pile elements at 6 in. (152 mm) elemental intervals.

The LPile and tri-linear constitutive behaviors of the soil springs used in the study are shown in Figure 3-7. As shown in the figure, the initial spring constant was found to be 800 kip/ft (11675 kN/m). The soil was modeled to behave linearly within a displacement limit of ± 0.75 in. (19 mm), after which the soil is expected to behave non-linearly. The results of the FE analysis that was carried out in this study showed that the displacement of these elements was well within the range of ± 0.75 in. (19 mm).

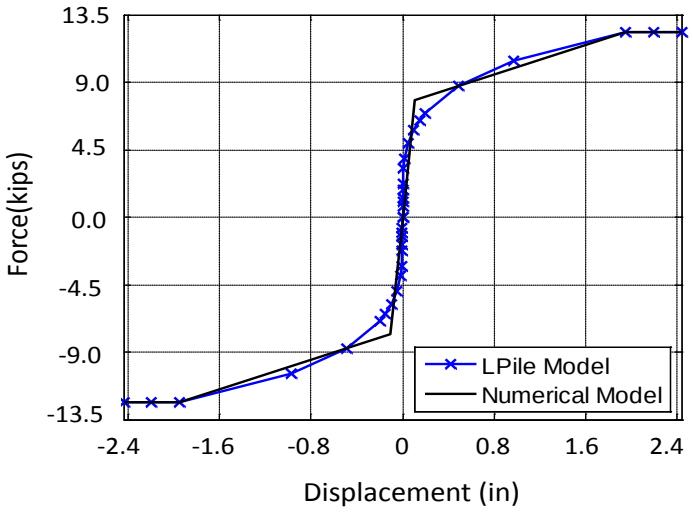

Figure 3-7. LPile and tri-linear numerical constitutive behaviors of the soil springs used in the study.

3.4.5 Application of Loads

The bridge model is subjected to two cases of loading for the bridge rating analysis: (1) dead load only, which includes the weight of the bridge components, and (2) vehicular live load only. The vehicular load used in this study was in accordance with the AASHTO Standard Specifications for Highway Bridges (AASHTO 2002). An HS20-44 vehicle was used as the design vehicle. The distance between the two rear axles was taken as 14 ft (4267 mm) in the model, keeping with AASHTO guidelines to obtain maximum effect on the deck. Based on the superstructure clear width, two trucks were positioned along two adjacent 12-ft (3658-mm)-wide lanes. To maximize the effect of eccentric compressive load on the piles, the two trucks should be placed such that the two lanes along only one span support the majority of the load. After several attempts, it was found that the critical position of the vehicles (shown in Figure 3-8) results in the lowest critical rating of the pile group supporting the interior bent, which was the center of focus in this study.

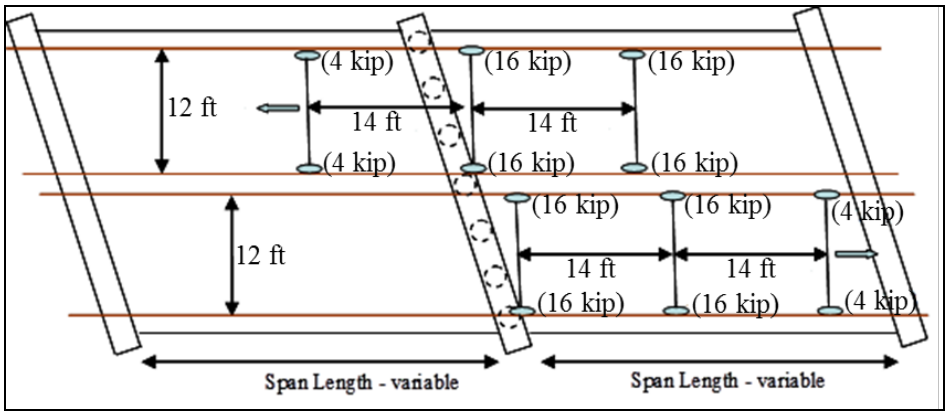

Figure 3-8. Plan of bridge deck with critical position of HS20-44 load.

3.5 PARAMETRIC STUDY METHODOLOGY

The effect of each of the geometric parameters of the two-span, simply supported bridge (span length, eccentricity of the deck, exposed pile length, and skew angle) on the modified critical structural rating of the timber pile group along Bent-2 (Figure 3-2) is studied for each of the deterioration profiles shown in Figure 3-1. Preliminary investigation was conducted using the two-factorial design of experiment method, which utilizes the analysis of variance (ANOVA) statistical technique (Walpole et al. 1998).

This investigation explored the impact of interaction between any two of the studied parameters on the rating of timber piles. However, the results of ANOVA showed that the effects of such an interaction on the critical rating are negligible. Therefore, it was deemed sufficient to study the effect of each parameter independent of the other parameters by varying the value of that particular parameter through the range shown in Table 3-1 while fixing the values of the other structural parameters at their respective average level. The rating analysis was done by changing the value of the relevant parameter in the finite element model of the prototype bridge.

The effect of deterioration on the pile rating was also studied using the deterioration profiles shown in Figure 3-1. The level of damage for each deterioration profile is increased, starting from an initial level of damage of 20% of the gross sectional area and increasing in intervals of 10%. This level of damage is increased to a level at which the structural rating obtained from the modified load rating procedure governs over the load rating based on the expected geotechnical capacity.

3.6 RESULTS OF PARAMETRIC STUDY

The parametric plots presented in Figures 3-9, 3-10, and 3-11 illustrate the variation of the critical load rating with respect to each of the four parameters for deterioration profiles I, II, and III, respectively, at various damage levels (%). Linear interpolation of values holds between two adjacent points of the parametric plot.

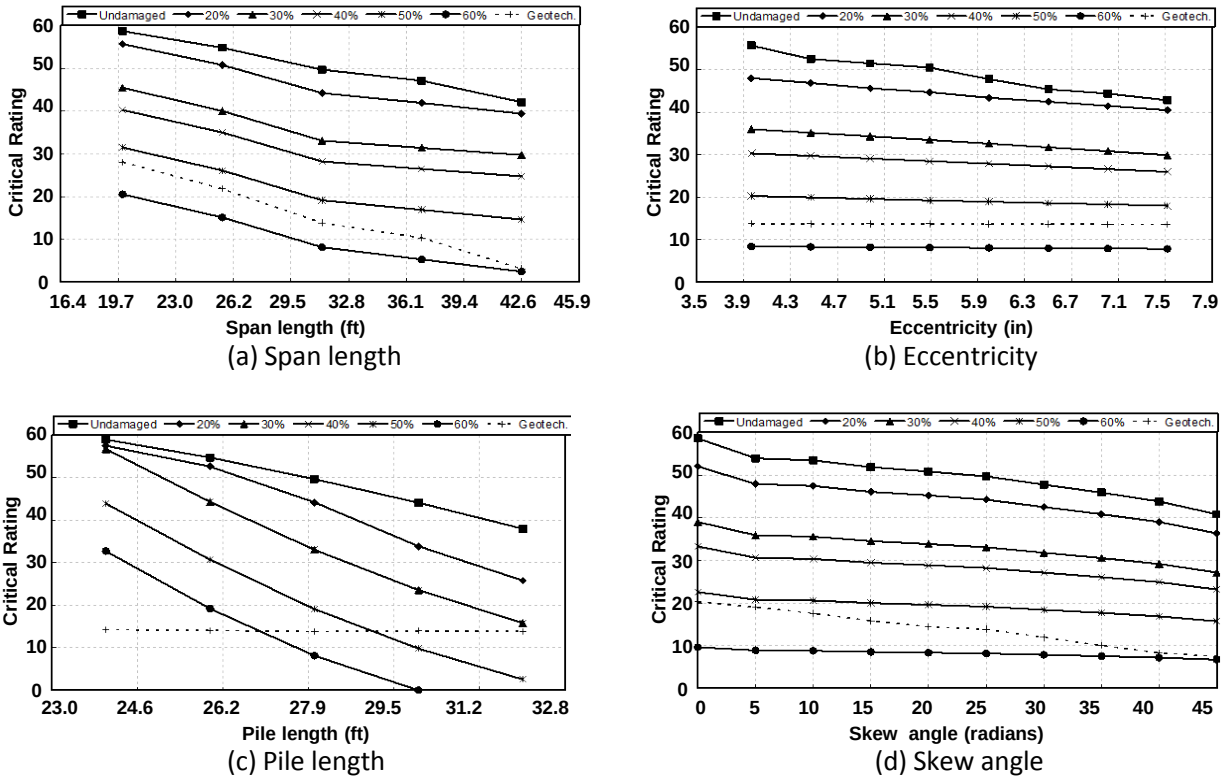

Figure 3-9. Parametric results of critical rating of timber piles with deterioration Profile I at various percentages of damage.

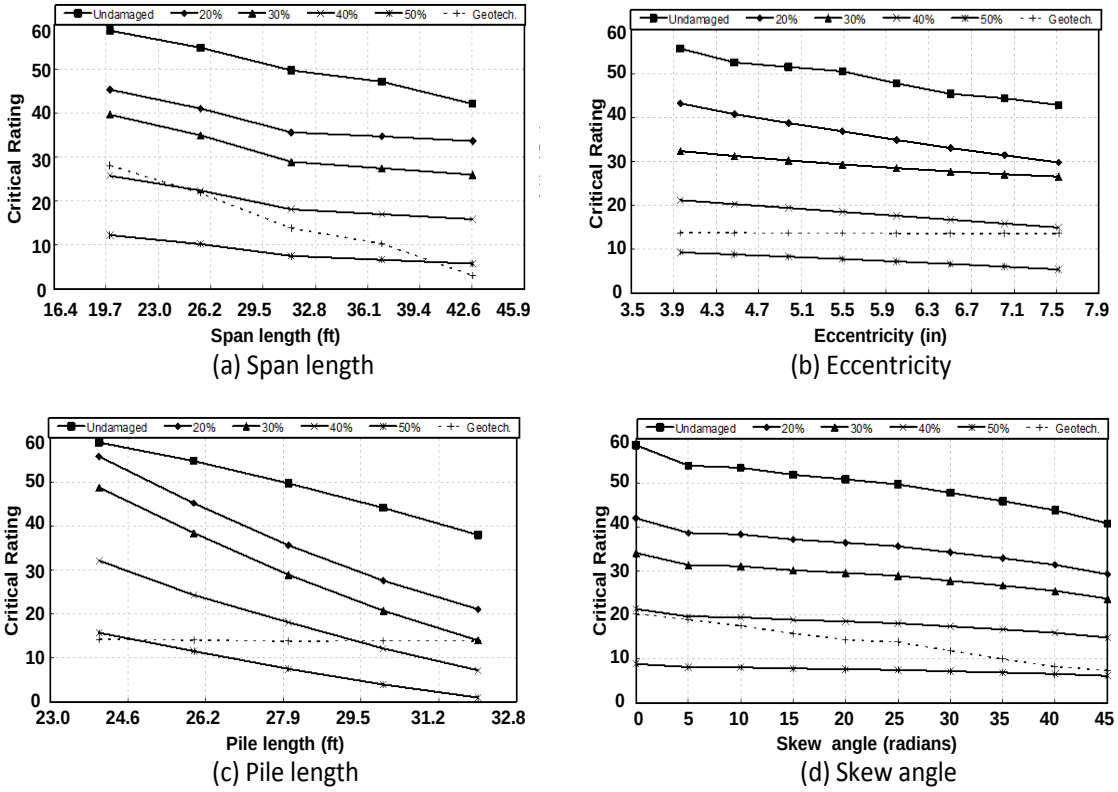

Figure 3-10. Parametric results of critical rating of timber piles with deterioration Profile II at various percentages of damage.

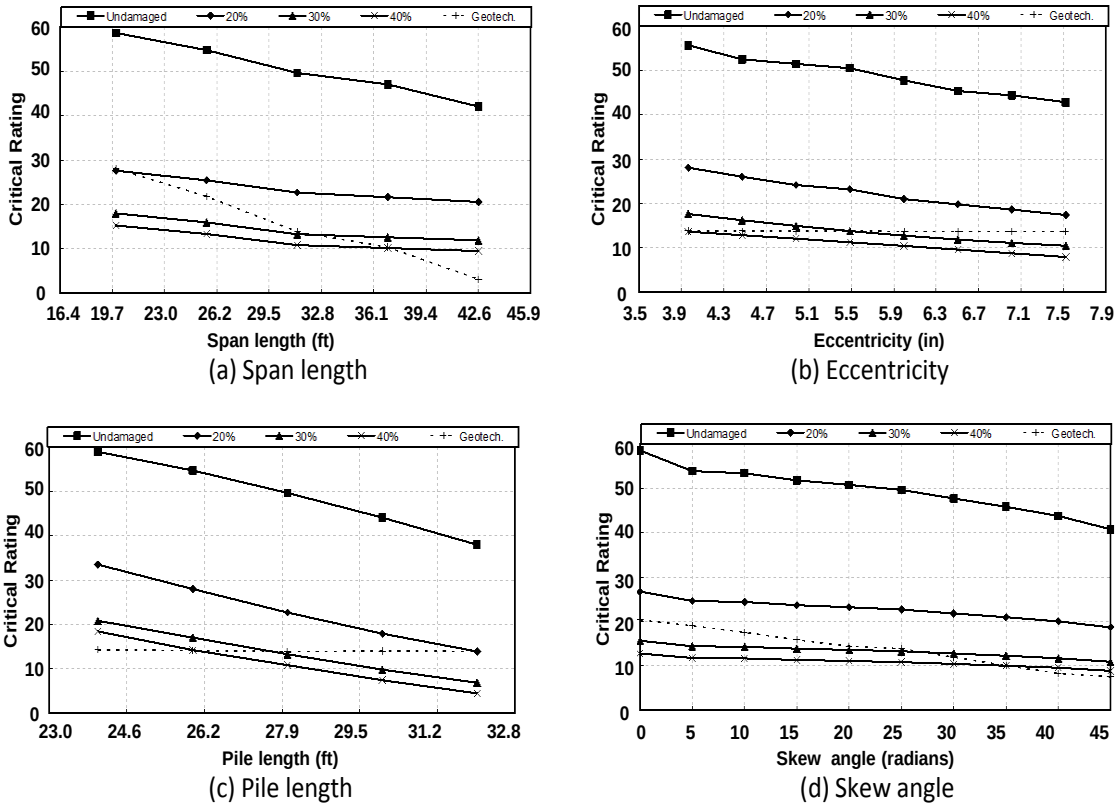

Figure 3-11. Parametric results of critical rating of timber piles with deterioration Profile III at various percentages of damage.

To facilitate the interpretation of the results presented in these figures, the data presented in the figures was fitted into the statistical linear regression model shown in Equation 3.1.

$$Y = \beta_o - \beta_1.X_1 - \beta_2.X_2 - \beta_3.X_3 - \beta_4.X_4 \quad (3.1)$$

where Y is the critical rating, X_1, X_2, X_3, and X_4 are normalized input parameters representing span length, eccentricity, exposed pile length, and skew angle, respectively, and β_o, β_1, β_2, β_3, and β_4 are the regression coefficients.

The input parameters were normalized using the average value of each parameter considered in the parametric study (Table 3-1). The values of the regression coefficients, which represent the impact of varying each parameter on the critical rating, are shown in Table 3-2 for the undamaged pile profile and the highest level of damage considered for each of the three deterioration profiles. It is worth noting that in all of the studied cases, the difference between the critical pile rating predicted from the regression model and that obtained from the FE analyses did not exceed 5%.

Table 3-2. Linear Regression Model Coefficients

Deterioration Profile	β_o	β_1	β_2	β_3	β_4
Undamaged	174.52	22.54	20.77	73.60	8.44
Profile I (60%)	155.04	25.31	0.92	118.56	1.0539
Profile II (50%)	76.15	9.10	6.36	51.74	1.21
Profile III (40%)	78.94	8.09	9.39	48.72	1.78

A careful examination of the plots presented in Figures 3-9, 3-10, and 3-11 reveals that the increase in the value of all four parameters considered in this study has negative impact on the critical rating of the piles; however, the level of impact varies depending on the studied parameter and the type of damage. By examining the results of the undamaged piles, which are common in all three figures, one can observe that within the range of values considered in this study, the reduction in the critical rating due to the increase of any of the four parameters did not exceed 35%, and this reduction was due to the increase of the pile length.

Figure 3-9, which presents the results of deterioration Profile I (Figure 3-1a) with damage levels varying from 20% to 60%, illustrates that the variation in the pile critical rating follows similar trends regardless of the level of damage. It also shows that for moderate levels of damage of this type (i.e., below 30%) the geotechnical-based concentric load rating governs over the eccentric load rating. The eccentric structural load rating, however, started to become more critical when the damage level reached 50%. Furthermore, from the slopes of the curves in all four plots presented in the figure, it can be concluded that the pile length parameter has the most severe effect on the critical rating among the four studied parameters. This is also confirmed by the regression coefficient values presented in Table 3-2, where the coefficient β_3 corresponding to pile length parameter for deterioration Profile I with 60% damage has the greatest value among all coefficients. Similarly, it can be concluded that for this damage type, the eccentricity has the least impact on the pile critical rating.

Figure 3-10 presents the results of deterioration Profile II (Figure 3-1b), with damage levels varying from 20% to 50%. The figure shows that the variation in the pile critical rating follows similar trends regardless of the level of damage. It also shows that for damage levels below 30%, the load rating based on the expected geometrical capacity governs over eccentric structural load rating. However, eccentric load rating becomes more critical when the damage level reached 40%, especially for longer piles. These observations indicate that deterioration Profile II is more critical compared to deterioration Profile I. This could be attributed to the eccentric distribution of the deterioration within the pile section that characterizes Profile II. Similar to the observations made about Figure 3-9, the slopes of the curves in all four plots presented in Figure 3-10, along with the regression coefficients presented in Table 3-2, suggest that the critical rating of piles with deterioration Profile II is most affected by the pile length parameter. As evidenced by its smallest regression coefficient value among all four

parameters, it can be concluded that for this type of damage, the skew angle has the least impact on the critical rating of piles.

Figure 3-11 presents the results of deterioration Profile III (Figure 3-1c) with damage levels varying from 20% to 40%. Although the figure shows that the variation in the pile critical rating follows similar trends regardless of the level of damage, it is clear that for this type of damage even a relatively minor damage will cause the rating value to decrease considerably. This was expected due to the conservative concentration of the damage in the compressive stress region of the pile section. The parametric results also show that eccentric structural load rating governs over load rating based on the expected geotechnical capacity for damage levels as low as 30%. These observations indicate that deterioration Profile III is more critical compared to deterioration Profiles I and II. The slopes of the curves in Figure 3-11 and the regression coefficients presented in Table 3-2 show that the critical rating of piles with deterioration Profile III is affected the most by the pile length parameter and the least by the skew angle.

CHAPTER 4 RETROFIT EXPERIMENTAL TESTING OF TIMBER PILES

Timber piles are susceptible to decay and deterioration that significantly impact the strength of the piles. To prolong the service life of the deteriorated pile, a retrofitting technique, often referred to as "posting," has been used in the United States. However, "posting" a pile jeopardizes its flexural capacity significantly. In this chapter, a retrofit technique is proposed using FRP to restore the flexural capacity of "posted" timber piles.

4.1 PROPOSED RETROFIT TECHNIQUE

Figure 4-1 shows schematics of the proposed retrofit technique that was adopted in this study. The first step is to align the timber post and the existing pile and connect them using a vertical steel drift pin at the center of the round pile (Figure 4-2a) or by using nails driven at the sides of the pile (Figure 4-2b).

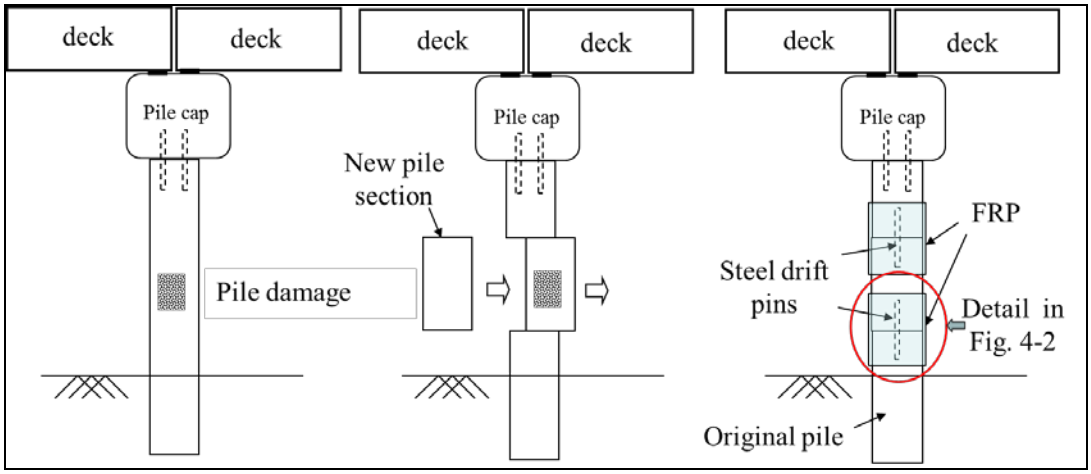

Figure 4-1. Proposed retrofit technique.

After the two spliced pieces of timber are attached, the round surface of the timber pile is sanded. A thin mortar shell [less than 0.5 in. (13 mm)] could be applied to provide a smooth round surface for the FRP sheets, which will be wrapped in the next step. Another advantage of using the mortar shell is to block any creosote oil that might be in the wood from contaminating the FRP resin. Finally, the FRP sheets are applied around the pile with resin using the hand lay-up process.

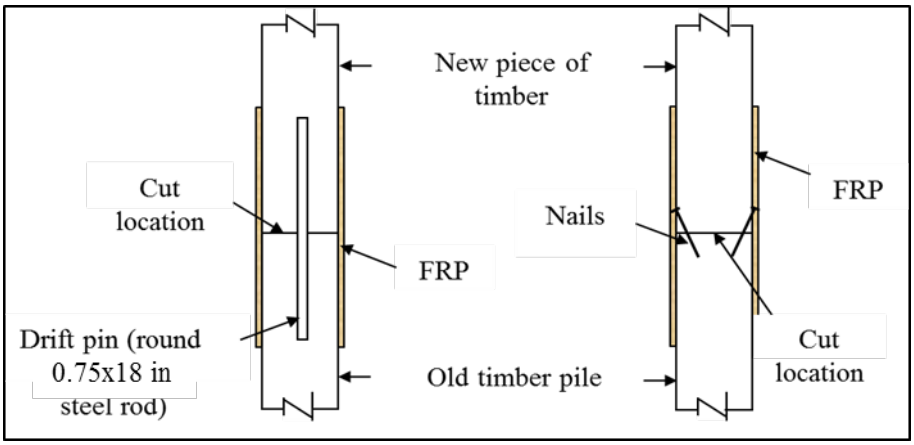

(a) Using a drift pin (b) Using nails

Figure 4-2. Detail of a post connection of a timber pile.

4.2 SPECIMEN DESCRIPTIONS

The experimental specimens used in this study were cut from pile samples retrieved from several bridges in Illinois. The retrieved samples varied in dimension (length and diameter) and age, which directly affected the level of deterioration in each specimen. It should be noted, however, that all timber piles had relatively moderate grades of decay. Figure 4-3 shows different types of decay observed in the tested specimens, including vertical cracks (Figure 4-3a), partially crushed fibers (Figure 4-3b), irregular shape of the section due to existence of a knot (Figure 4-3c), and cracks filled with mold and fungus (Figure 4-3d).

(a) (b) (c) (d)

Figure 4-3. Types of decay observed in the tested pile specimens: (a) vertical crack, (b) partially crushed fibers, (c) irregular shape, and (d) mold and fungus inside of cracks.

In total, twenty specimens were prepared by cutting them from the retrieved piles. The specimens were cut to a constant length of 48 in. (1.22 m), and their diameter varied between 9.8 in. (249 mm) and 13.4 inch (340 mm). Four of them were tested

under compression only, and the other sixteen under compression flexure. Each specimen was tested twice. The purpose of the tests was to determine the strength and stiffness of the unretrofitted and retrofitted timber piles. For the compression-flexure tests, the specimen was cut perpendicular to its longitudinal axis in two equal halves, and the two halves were spliced together using the proposed retrofit technique (i.e., with a steel drift pin or nails and FRP sheets). The specimen test matrix is summarized in Table 4-1a for the compression-only tests and Table 4-1b for the compression-flexure tests. The nomenclature used for the unretrofitted and retrofitted specimens under compression only is SPxU-C and SPxR-C, respectively. For the compression-flexure tests, the nomenclature is SPxU and SPxR, respectively, where "x" indicates the specimen number.

Table 4-1a. Specimen Test Matrix (Compression-Only Tests)

Specimen	D [in. (mm)]	Retrofit Details
SP1-C	13.4 (340)	GFRP
SP2-C	12.7 (323)	CFRP, mortar shell
SP3-C	11.7 (297)	GFRP
SP4-C	10.9 (277)	GFRP, mortar shell

Table 4-1b. Specimen Test Matrix (Compression-Flexure Tests)

Specimen	D [in. (mm)]	Retrofit Details
SP1	10.3 (262)	GFRP
SP2	11.4 (290)	GFRP
SP3	9.8 (249)	GFRP
SP4	11.1 (282)	GFRP
SP5	10.3 (262)	GFRP
SP6	10.9 (277)	GFRP
SP7	10.0 (254)	GFRP
SP8	12.5 (318)	GFRP, mortar shell
SP9	12.0 (305)	CFRP, mortar shell
SP10	12.4 (315)	GFRP, mortar shell
SP11	12.2 (310)	GFRP, mortar shell
SP12	12.5 (318)	GFRP, wedge
SP13	11.5 (292)	CFRP, wedge
SP14	10.2 (259)	GFRP, nails
SP15	11.4 (290)	GFRP, nails
SP16	12.5 (318)	GFRP, nails

It is important to note that one of the specimens (SP2-C in Table 4-1a), as well as two of the sixteen specimens (SP9 and SP13 in Table 4-1b), were retrofitted with carbon FRP (CFRP) sheets, while the other specimens were wrapped with GFRP sheets.

To examine the effect of using mortar shell prior to wrapping the FRP sheets, a mortar shell was utilized in the retrofit of specimens SP2-C, SP4-C, SP8, SP9, SP10, and SP11. For the compression-flexure specimens, to explore the effect of the presence of excessive decay and cavities in the piles, a wedge was introduced in two of the specimens (SP12 and SP13). As shown in Figure 4-4, the wedge was introduced by cutting out a portion of the pile and filling it with mortar prior to FRP wrapping. Furthermore, because the use of center-lined drift pins to align the two spliced timber pieces could be problematic in the field, the possibility of using diagonally driven nails at the sides of the specimen was examined in three specimens (SP14, SP15, and SP16). Figure 4-5 presents pictures of the procedures used in preparing the flexure-compression specimens.

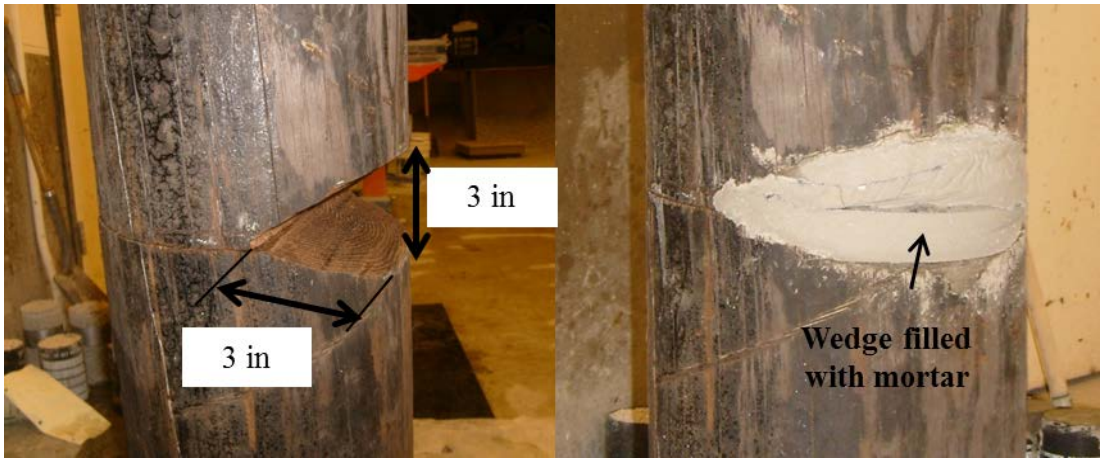

Figure 4-4. Wedge at the post connection.

The materials shown in Table 4-2a were used for the four specimens tested in compression only. Table 4-2b summarizes properties and details of the materials used in retrofitting the specimens subjected to compression flexure. As shown in the tables, the materials that had the best structural behavior in the compression-only tests were again used for the compression-flexure tests, except in the case of the CFRP. The carbon fabric used in the compression-flexure tests was plain weave, which is characterized by light weight and high stiffness. Vinylester resin formed the matrix of both GFRP and CFRP. The glass fabric was woven roving. It was selected for its relatively inexpensive, high impact, and high strength two-directional reinforcement properties. The concrete mortar used in this study consisted of Portland cement and bonding agents to accelerate gain and set time. A wide range of FRP materials was used in the compression-only tests, as can be seen in Table 4-2a, to explore their effectiveness for timber pile retrofit.

(a) Pile cut

(b) Steel pin installation

(c) Sanding

(d) Mortar shell

(e) FRP wrapping

Figure 4-5. Details of the pile retrofit procedure.

Table 4-2a. Material Employed to Retrofit the Piles Tested in Compression Only

Material	**Properties**	**Test**
Glass FRP	E = 2700 ksi (18600 MPa), thickness 0.0043 in. (0.1 mm)	1,4
Glass FRP	E = 1800 ksi (12400 MPa), thickness 0.025 in. (0.6 mm)	3
Carbon FRP	E = 19694 ksi (135800 MPa), thickness 0.014 in. (0.4 mm), unidirectional	2
Epoxy resin	Medium viscosity, light amber resin	1,4
Polyester resin	Wax-free, general-purpose resin	2,3
Epoxy hardener	120 minutes pot life	1,4
Hardener	MEKP 1% by weight	2,3
Concrete mortar	Compressive strength (1 day) = 3 ksi (22 MPa), final set time of 2 hr	2,4

Table 4-2b. Properties of the Materials Used to Retrofit the Piles Tested in Compression-Flexure

Material	**Properties**
Glass FRP	E = 1800 ksi (12400 MPa), thickness = 0.025 in. (0.6 mm)
Carbon FRP	E = 19694 ksi (135800 MPa), thickness = 0.012 in. (0.3 mm)
Concrete mortar	Compressive strength (1 day) = 3 ksi (22 MPa), final set time of 2 hr

4.3 TEST SET-UP

The tests performed in this study were conducted using a 600 kip (2670 kN) MTS uniaxial servo-controlled compression machine. The actuator was controlled using an INSTRON 8800 controller. The testing frame contained an internal 600 kip (2670 kN) load cell and an internal linear variable differential transducer (LVDT) to measure actuator position.

For the compression-only tests, the specimens were instrumented with two extensometers 180° apart to measure axial strain, and a perimeter extensometer to measure circumferential strains. For the compression- flexure tests, the specimens were also instrumented with two vertical extensometers placed at the mid-height of the specimen on two opposite sites to measure axial strains (Figure 4-6).

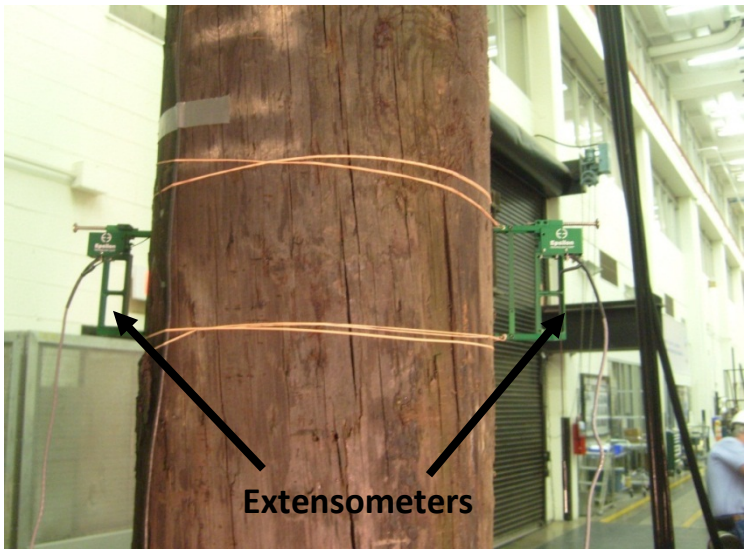

Figure 4-6. Longitudinal extensometers on both sides of the specimen.

Two additional LVDTs were located at the top and bottom of a pile specimen to monitor the relative displacement between the specimen and the end plates during

testing. The typical disposition of the LVDT located at the top of the pile is shown in Figure 4-7.

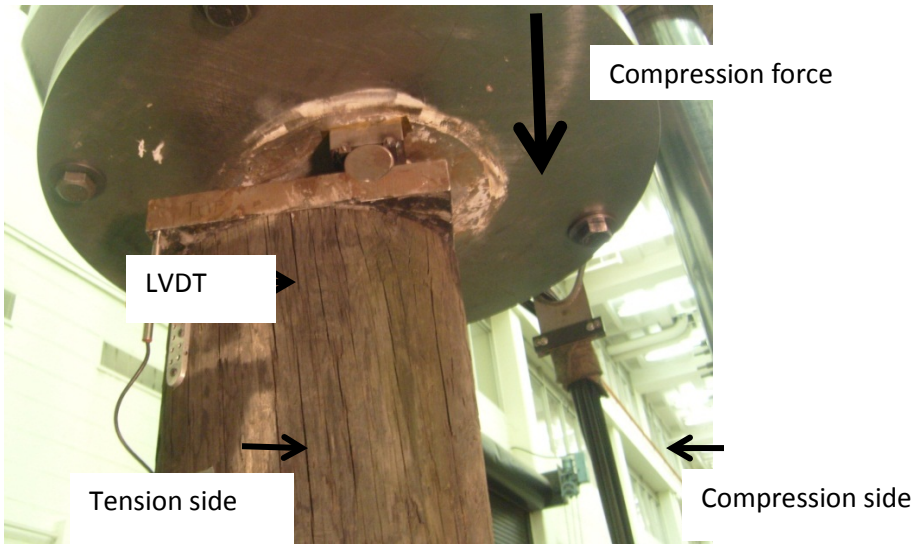

Figure 4.-7. Installed LVDT at the top of the pile.

Special fixture plates were designed, manufactured, and mounted at both ends of the specimen to apply the axial load eccentrically in the compression-flexure tests. The specimens were bolted to 1-1/2 in. (38 mm) thick steel plates on each end using ten 3/4 in. × 6 in. (19 mm × 152 mm) bolts for the top plate and eight 3/4 in. × 6 in. (19 mm × 152 mm) bolts for the bottom plate. Figure 4-8 shows schematics of the special plates used for applying the eccentric load.

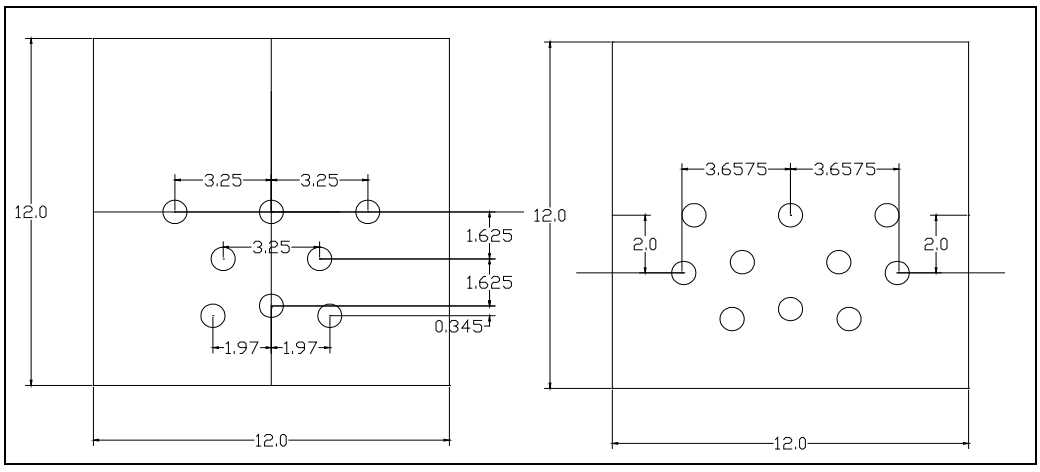

(a) Bottom plate (b) Top plate

Figure 4-8. Steel fixture plates used to apply eccentric axial load on the specimens tested in compression-flexure (dimensions in inches).

The plates were loaded through 2 in. (51 mm) rollers that were placed a distance of 3 in. (76 mm) from the centroidal axis of the pile specimen (Figure 4-9). Figure 4-10 shows an installed specimen in the 600 kip (2670 kN) machine frame.

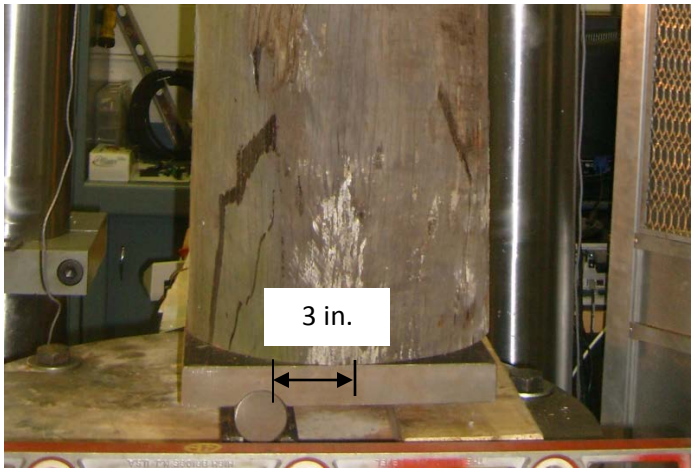

Figure 4-9. Typical roller at the base of the pile.

Figure 4-10. An installed specimen on the MTS testing machine.

Both types of loading, compression-only and flexure-compression, were conducted under monotonic displacement control at a cross-head rate of 0.05 in. (1.3 mm) per minute. First, an unretrofitted specimen was tested until a point where non-linear behavior of the specimen was observed. The maximum load recorded at this point was considered the elastic strength of the pile specimen.

4.4 ELASTIC DESIGN OF FRP WRAPS

To determine the number of FRP layers needed for the retrofitting of the piles tested in compression-flexure, an elastic design procedure was adopted. The procedure was based on the assumption that at the interface section between the new section and the old pile, the tensile stresses are resisted entirely by the FRP and the compressive stresses are resisted by both wood and FRP. At the retrofitted section, the portion of the wood resisting compression is called "effective area" (Figure 4-11).

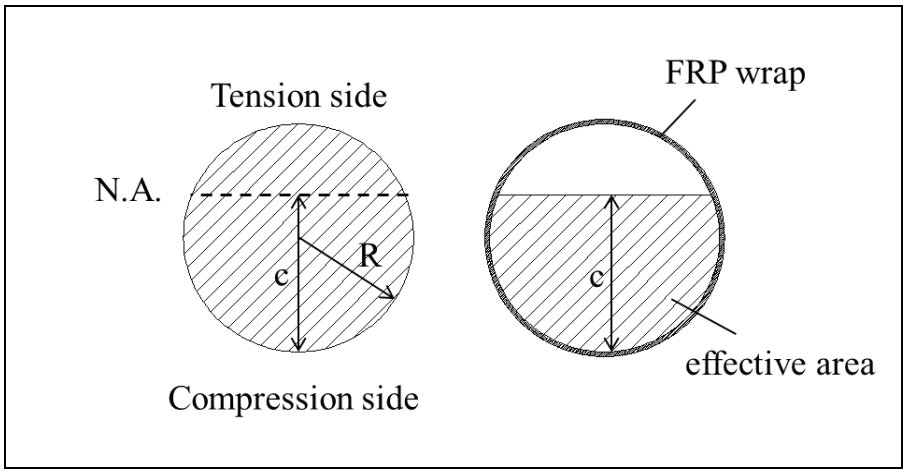

(a) Original section (b) Retrofitted section

Figure 4-11. Original vs. retrofitted section at the post connection interface.

To determine the number of FRP layers that gives the same flexural stiffness in the retrofitted pile as that of the unretrofitted pile, the following formula was used:

$$E_{Wood}I = E_{Wood}I_{comp} + E_{FRP}I_{FRP} \quad (4\text{-}1)$$

where E_{Wood} is the modulus of elasticity of wood, I is the moment of inertia of the complete circular section of the original pile, I_{comp} is the moment of inertia of the effective area of the pile section (Figure 4-11), E_{FRP} is the modulus of elasticity of FRP, and $I_{FRP}$is the moment of inertia of the FRP wraps used for retrofitting the timber pile.

Equation 4-1 was used to derive the equation for computing the required FRP volumetric ratio, ρ_{FRP}, which is defined as the ratio between the FRP and timber volumes. The volumetric ratio of FRP can be expressed as $[(D + 2nt)^2 - D^2]/D^2$, where D is the diameter of the pile, n is the number of FRP layers, and t is the thickness of a FRP layer. Using Equation4-1, the volumetric ratio of FRP can be described as:

$$\rho_{FRP} = -1 + \sqrt{1 + \left(1 - \frac{I_{comp}}{I}\right)\frac{E_{Wood}}{E_{FRP}}} \tag{4-2}$$

Additionally, Equation 4-2 can be rewritten in terms of the required number of FRP layers as follows:

$$n = \frac{D}{2t}\left(\left(1 + \left(1 - \frac{I_{comp}}{I}\right)\frac{E_{Wood}}{E_{FRP}}\right)^{\frac{1}{4}} - 1\right) \tag{4-3}$$

The moment of inertia of the effective area of the timber pile section is calculated from the following equation:

$$I_{comp} = \pi\frac{R^4}{8} + \frac{y_1^*}{2}\sqrt{\left(R^2 - y_1^{*2}\right)^3} - \frac{R^2}{4}\left[y_1^*\sqrt{R^2 - y_1^{*2}} + R^2\sin^{-1}\left(\frac{y_1^*}{R}\right)\right];$$
$$R = \frac{D}{2}; \qquad y_1^* = R - c \tag{4-4}$$

where c is the depth of the effective area of the timber pile section (Figure 4-11). Note that c can be calculated from the classical equation for elastic stresses (Ambrose and Tripeny 2009; Buchanan 1986):

$$c = \frac{D}{2} + \frac{I}{Ae} \tag{4-5}$$

where A is area of the circular section of the pile, and e is eccentricity.

Figure 4-12 shows an example of the strain distribution at the interface determined from the tests using the two extensometers attached on both sides of the specimen. In this figure, compressive strains are considered negative and tensional strains positive. The presented distributions are for the unretrofitted (SP4U) and

retrofitted (SP4R) specimen 4. Using the experimental strain data, the depths of the effective area of SP4R and SP4U were found to be 7.9 in. (201 mm) and 8.6 in. (218 mm), respectively, with a difference of 7.8%. For comparison, the analytical depth of the effective area was also computed using Equation 4-5 and was found to be 8.1 in. (206 mm); hence, the differences between the analytical and experimental *c* values of the retrofitted and unretrofitted specimens were approximately 2.5% and 5.8%, respectively. This minor difference could possibly be due to imperfections in the piles' circular section and decay and damage of the wood.

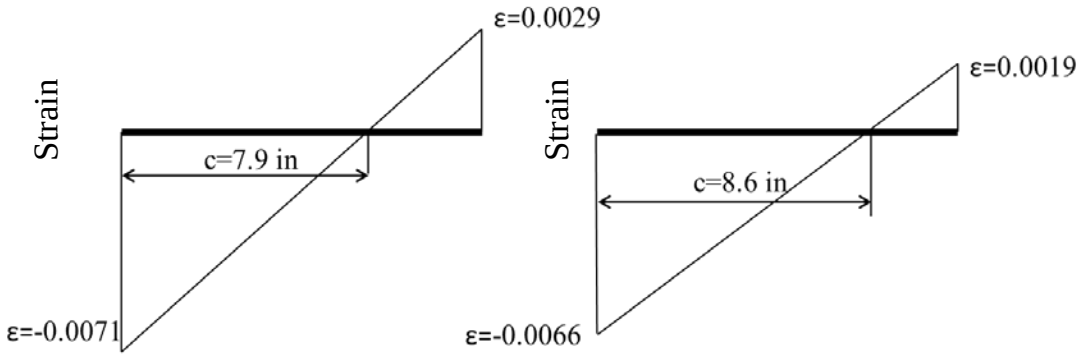

(a) SP4R (b) SP4U

Figure 4-12 Depth of the effective area, *c*, in SP4 [*D* = 11.1 in. (282 mm)].

The diameter of the section of the timber piles (D) subjected to compression-flexure varied between 9.8 inch (249 mm) and 12.5 in, correspondingly I_{comp} / I varied between 0.55 and 0.61. If the mean value for I_{comp} / I (i.e. 0.58) is used, Equation 4-2 can be further simplified to

$$\rho_{FRP} = -1 + \sqrt{1 + 0.42 \frac{E_{Wood}}{E_{FRP}}} \tag{4-6}$$

Equation 4-6 shows that the ratio E_{Wood} / E_{FRP} is the key factor governing the design of FRP, but the modulus of elasticity of wood and FRP can vary substantially.

As shown in Table 4-2b, the modulus of elasticity of GFRP and CFRP used in this study was 1800 ksi (12400 MPa) and 19694 ksi (135800 MPa), respectively, and the modulus of elasticity of the wood was determined experimentally using the results of the tests conducted on unretrofitted specimens. Based on the results of the sixteen tested specimens under compression-flexure, the mean value of the modulus of elasticity of wood was found to be 649 ksi (4477 MPa) with the standard deviation of 179 ksi (1234 MPa). In addition, there is a 95% confidence that the true value of the modulus of elasticity is between 554 ksi (3820 MPa) and 745 ksi (5136 MPa). The National Design

Specification for Wood Construction recommends the following values for modulus of elasticity of treated round timber piles for normal load duration and wet service conditions of northern and southern red oak: E = 1250 ksi (8618 MPa) and E_{min} = 660 ksi (4550 MPa). To be on the conservative side, the value of E_{min} was chosen as the modulus of elasticity for timber in the pile retrofit tests; that value was also chosen because it is close to the mean value and within 95% confidence interval of the experimental values.

Table 4-3a contains compression-only specimens. The number of layers and/or FRP volumetric ratios shown in this table were determined by trial and error such that the retrofitted capacity of the timber pile would be higher than the unretrofitted case.

Table 4-3a. Number of Experimentally Used FRP Layers
(Compression-Only Tests)

	SP1-C	**SP2-C**	**SP3-C**	**SP4-C**
# of FRP layers	9	2	10	9
ρ_{FRP}	0.0131	0.0090	0.0708	0.0276

On the other hand, and based on the design procedure described above, the number of FRP layers used for compression-flexure specimens was calculated and is summarized in Table 4-3b. The first row in that table corresponds to the number of FRP layers predicted using Equation 4-3, while the second row corresponds to the number of layers actually used in the tests. The last row shows the FRP volumetric ratio (ρ_{FRP}). As shown in the table, a number of layers similar to or greater than the number predicted by Equation 4-3 was utilized for retrofitting specimen SP1 and specimens SP8 through SP13. However, because most of these tests showed that the retrofitted specimens could reach higher strength than that of the unretrofitted specimens and to optimize the design of the FRP sheets, using a smaller number of layers than those computed based on Equation 4-3 was also considered. It is important to point out that the CFRP volumetric ratios used for SP9 and SP13 are much smaller than those of the GFRP retrofitted specimens. This is due to the significantly higher modulus of elasticity of CFRP compared to GFRP.

Table 4-3b. Number of FRP Layers (Flexure-Compression Tests)

		SP1R	**SP8R**	**SP9R**	**SP10R**	**SP11R**	**SP12R**	**SP13R**	**SP2R**
No. of FRP layers	Equation 4-3	8	9	2	9	9	9	2	9
	Test	8	9	2	10	9	9	2	7
ρ_{FRP}	Test	0.079	0.074	0.008	0.084	0.076	0.073	0.008	0.062

		SP3R	**SP4R**	**SP5R**	**SP6R**	**SP7R**	**SP14R**	**SP15R**	**SP16R**
No. of FRP layers	Equation 4-3	8	9	8	8	8	8	9	9
	Test	6	7	6	6	6	6	6	7
ρ_{FRP}	Test	0.062	0.064	0.059	0.056	0.061	0.060	0.053	0.057

CHAPTER 5 EXPERIMENTAL TEST RESULTS

5.1 COMPRESSION-ONLY TESTS

This series comprises only four unretrofitted/retrofitted specimens. These tests helped tune the materials and equipment to be used in the compression-flexure tests, as well as to confirm that the employed FRP retrofit technique was capable of producing strengths similar to those observed in the unretrofitted specimens. The principal results are summarized in Table 5-1.

Table 5-1. Experimental Results for Compression-Only Tests

Test	**SP1-C**	**SP2-C**	**SP3-C**	**SP4-C**
P_{unret} [kips (kN)]	551 (2451)	180 (801)	331 (1472)	214 (952)
P_{ret} [kips (kN)]	452 (2010)	276 (1228)	500 (2224)	151 (672)
P_{ret}/ P_{unret}	0.82	1.53	1.51	0.71

In Table 5-1, the first and second rows, P_{unret} and P_{ret}, correspond to the maximum compression force of the unretrofitted and retrofitted specimens, respectively. The last row corresponds to the ratio between retrofitted and unretrofitted maximum forces. Specimens SP1-C and SP4-C experienced early local failure of the GFRP. In contrast, specimen 3-C, with a higher GFRP volumetric ratio, had a higher P_{ret}/ P_{unret} ratio. Specimen 2-C, which was retrofitted using CFRP, also showed a high retrofitted force compared to the unretrofitted force.

5.2 COMPRESSION-FLEXURE TESTS

The results of the flexure-compression tests of all sixteen pile specimens are summarized in Table 5-2. The table is divided into four sections based on the retrofit details used for the specimens. The specimens were retrofitted as follows: (1) with FRP sheets without mortar shell, (2) with FRP sheets and mortar shell, (3) with FRP sheets and mortar-filled wedges, and (4) with only FRP sheets but the pile was connected using nails, while other specimens listed in previous sections were connected using steel drift pins (Figure 4-2). The first and second rows in each section of the table represent the maximum compression forces of the unretrofitted (P_{unret}) and retrofitted (P_{ret}) specimens, respectively. The third row presents the ratio between retrofitted and unretrofitted maximum forces. It is important to highlight specimens such as SP8 and SP16 that have the same size and yet different strengths due to different amounts of deterioration and defects in the wood.

Table 5-2. Maximum Forces of Unretrofitted and Retrofitted Specimens Under Flexure-Compression Tests

Without Mortar Shell							
Specimen	**SP1**	**SP2**	**SP3**	**SP4**	**SP5**	**SP6**	**SP7**
P_{unret} [kip (kN)]	78 (347)	98 (436)	65 (289)	194 (863)	116 (516)	127 (565)	73 (325)
P_{ret} [kip (kN)]	87 (387)	119 (529)	74 (329)	205 (912)	105 (467)	127 (565)	73 (3253)
P_{ret}/ P_{unret}	1.12	1.21	1.14	1.06	0.91	1.00	1.00
With Mortar Shell							
Specimen	**SP8**	**SP9**	**SP10**	**SP11**			
P_{unret} [kip (kN)]	316 (1406)	177 (787)	125 (555)	153 (681)			
P_{ret} [kip (kN)]	314 (1397)	175 (778)	153 (681)	182 (810)			
P_{ret}/ P_{unret}	0.99	0.99	1.23	1.19			
With Wedge							
Specimen	**SP12**	**SP13**					
P_{unret} [kip (kN)]	133 (592)	163 (725)					
P_{ret} [kip (kN)]	180 (801)	81 (360)					
P_{ret}/ P_{unret}	1.35	0.50					
With Nails							
Specimen	**SP14**	**SP15**	**SP16**				
P_{unret} [kip (kN)]	68 (302)	112 (498)	142 (632)				
P_{ret} [kip (kN)]	79 (351)	112 (498)	140 (623)				
P_{ret}/ P_{unret}	1.16	1.00	0.99				

The maximum forces attained in the retrofitted tests were similar to or greater than those obtained from the unretrofitted specimens regardless of the retrofitting details, with the exceptions of specimens SP5 and SP13. The strength of the retrofitted specimen SP5 was 91% of that of the unretrofitted specimen. This slight reduction in strength could possibly be due to imperfectly wrapped FRP sheets because the surface of the specimen was quite uneven. Note that the specimens with mortar shell, which made the

surface of the specimens more evenly round, showed no reduction in strength. For SP13, due to the weak out-of-plane resistance of the CFRP jacket, an early crushing was observed of the filling material (mortar) in the wedge cut between the two halves of the timber pile specimen. This weakness was produced by the extremely small thickness of the CFRP jacket. Further, the results shown in the table prove that using steel drift pins or nails produces similar performance: the average $P_{ret}/\ P_{unret}$ ratio for these cases were 1.06 and 1.05, respectively.

To better understand how the behavior of retrofitted specimens tested in compression-flexure compares to that of unretrofitted specimens, some selected force-displacement relationships for different retrofit details are presented in Figure 5-1. In this figure, the displacements are obtained from the internal LVDT of the compression machine [i.e., the displacements at the point of application of the compression load, 3 in. (76 mm) away from the centroid of the pile circular section]. Early in the loading history, up to approximately 20 kips, both unretrofitted and retrofitted specimens had a softer behavior, in all cases, likely due to the flexibility of the loading frame. The retrofitted test was subsequently slightly softer than the unretrofitted test for the cases shown in Figure 5-1a and Figure 5-1d. This behavior is likely due to the slight damage exerted on the specimen when it was first tested, while it was still unretrofitted.

Moreover, it was found that the use of mortar shell with FRP sheets helped restore the strength and stiffness of the pile (Figure 5-1b). Hence, using mortar shell could be recommended when piles have higher levels of damage. In the case where a mortar-filled wedge is introduced prior to wrapping the specimen with FRP, since the elastic modulus of mortar was higher than the elastic modulus of the wood, the retrofitted pile showed higher stiffness than that of the unretrofitted pile at the initial stage (Figure 5-1.c). However, as the testing progressed, the specimen became softer due to the weak out-of-plane resistance of the CFRP jacket, as mentioned earlier, which provided very little confinement for the filling mortar, resulting in its early crushing. As shown in Figure 5-1d, using nails or drift pins does not significantly impact the capacity or stiffness of the retrofitted piles.

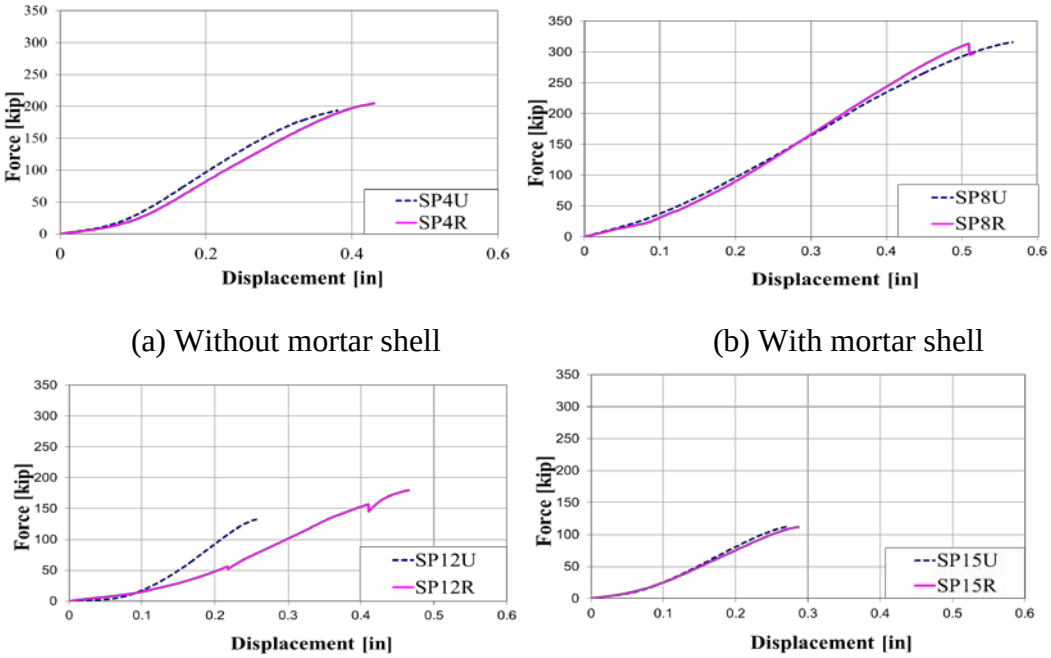

(a) Without mortar shell (b) With mortar shell

(c) With wedge (d) With nails

Figure 5-1. Force-displacement relationship for specimens with different retrofit conditions.

In an elastic design of the pile cap and piles, forces are distributed from the pile cap to the piles according to the stiffness of each pile because the pile cap can be regarded as a rigid body. If one pile is less rigid than others, then those piles will be overloaded. Furthermore, excessive displacements could produce additional P-delta effects and further reductions in the capacity of the timber pile. Therefore, it was important to ensure that, although the strength of the retrofitted specimens was satisfactory, their stiffness is not significantly impacted. To eliminate the effect of early hardening, highlighted earlier in this discussion, the stiffness was calculated after the specimen reaches a stable linear behavior. It was found by inspection that this behavior occurs approximately between one third and two thirds of the maximum force. Figure 5-2 shows an example of computing stiffness for specimen SP8.

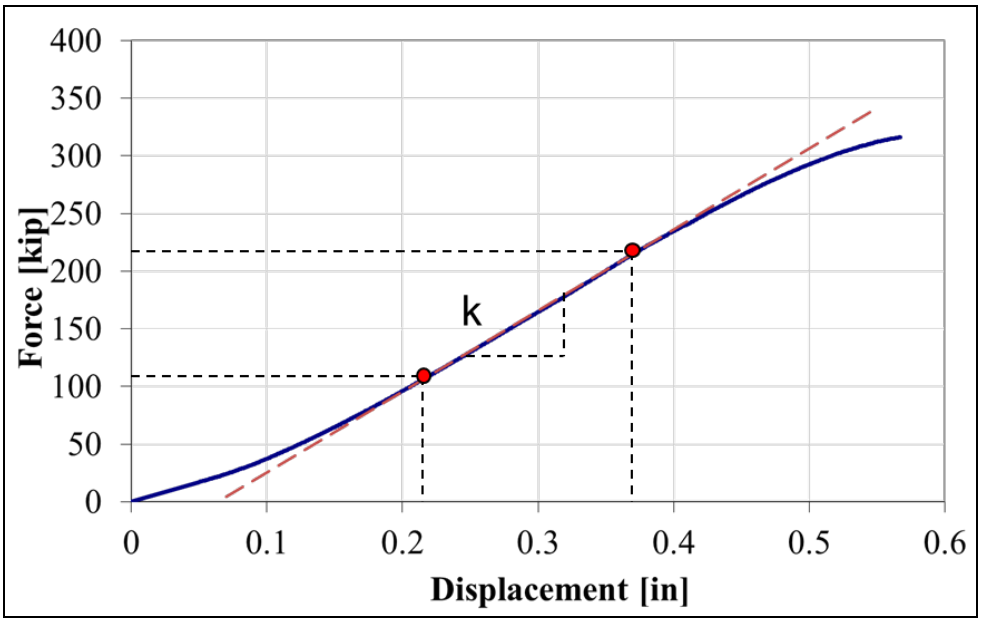

Figure 5-2. Timber pile stiffness (SP8).

A comparison between the unretrofitted and retrofitted stiffness of each specimen is presented in Figure 5-3. The results of CFRP retrofitted specimens are excluded in Figure 5-3 because SP13 showed a different type of failure mechanism and because the results produced higher standard deviation when added to the GFRP test results; hence, it was more conservative to eliminate them. SP11 was not presented either because it experienced relatively extensive damage during the unretrofitted test.

The retrofitted specimens SP1, SP2 and SP8 show higher stiffness than that of the unretrofitted specimens, as evidenced by the extremely minor damage shown by those specimens during the unretrofitted test. By using mortar shell, the stiffness of the retrofitted specimens was fully restored, and the stiffness of specimens SP8R and SP10R was found to be 112% and 99% of the unretrofitted specimens, respectively. The stiffness results presented in Figure 5-3 show a mean stiffness reduction of 5% and median stiffness reduction of 14% for the retrofitted specimens compared with the unretrofitted specimens.

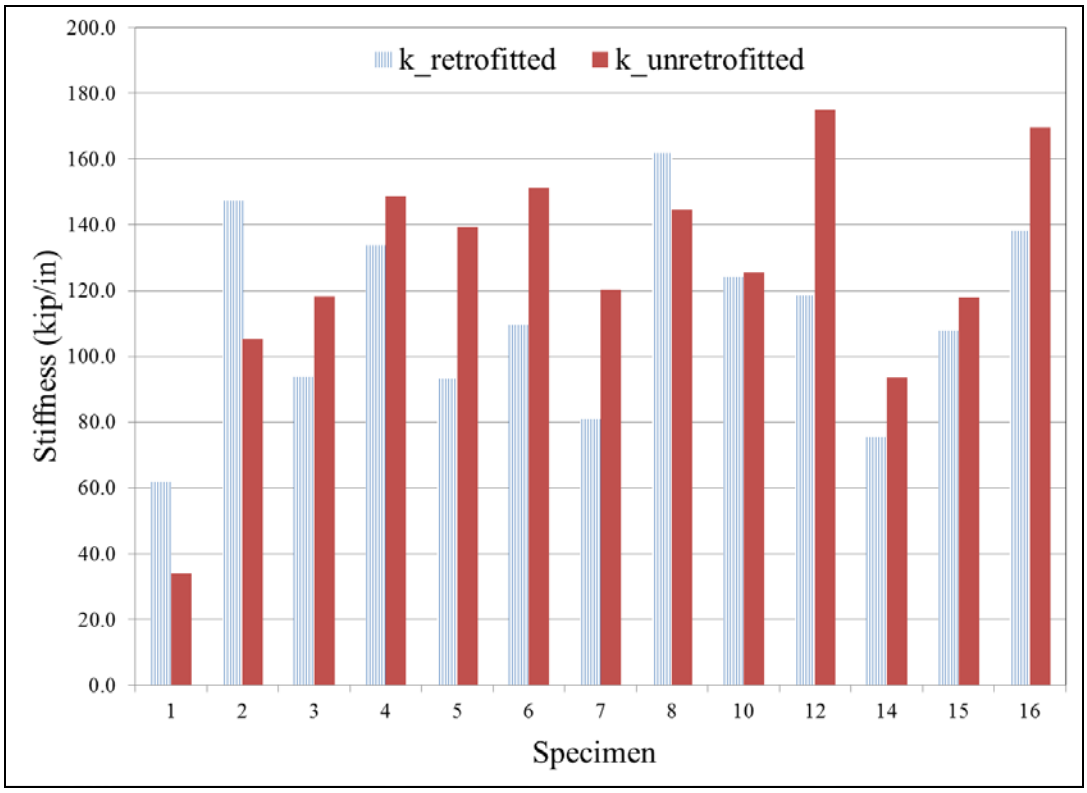

Figure 5-3. Stiffness (kip/in.) for unretrofitted and retrofitted specimens.

5.3 DESIGN RECOMMENDATIONS

Figure 5-4 shows a graph of the ratios of the maximum retrofitted forces to the maximum unretrofitted forces with respect to the GFRP volumetric ratio used for the retrofitted specimens. A linear regression analysis was conducted and the result is shown as a solid straight line in the figure. The two dashed lines drawn in the figure represent $\mu \pm 2\sigma$ where, μ is the mean and I? is the standard deviation of the data points. As shown in the figure, only two data points lie below the lower dashed line; hence, it was deemed appropriate to base the design on the $\mu \pm 2\sigma$ value. The design point is considered when the $\mu \pm 2\sigma$ line intersects the horizontal line corresponding to a ρ_{ret}/ρ_{unret} ratio equal to 1.0. Therefore, the design volumetric ratio of GFRP is found to be 0.068. Note that only the tests with GFRP were used to calculate the results shown in Figure5-4. It is important to note also that the 1.08 is the average ratio of the retrofitted to the unretrofitted stiffnesses of the five specimens whose volumetric ratios were higher than the proposed value of 0.068. This confirms that, while similar strength can be expected by using the proposed volumetric ratio, the stiffness of the retrofitted specimens will not be jeopardized.

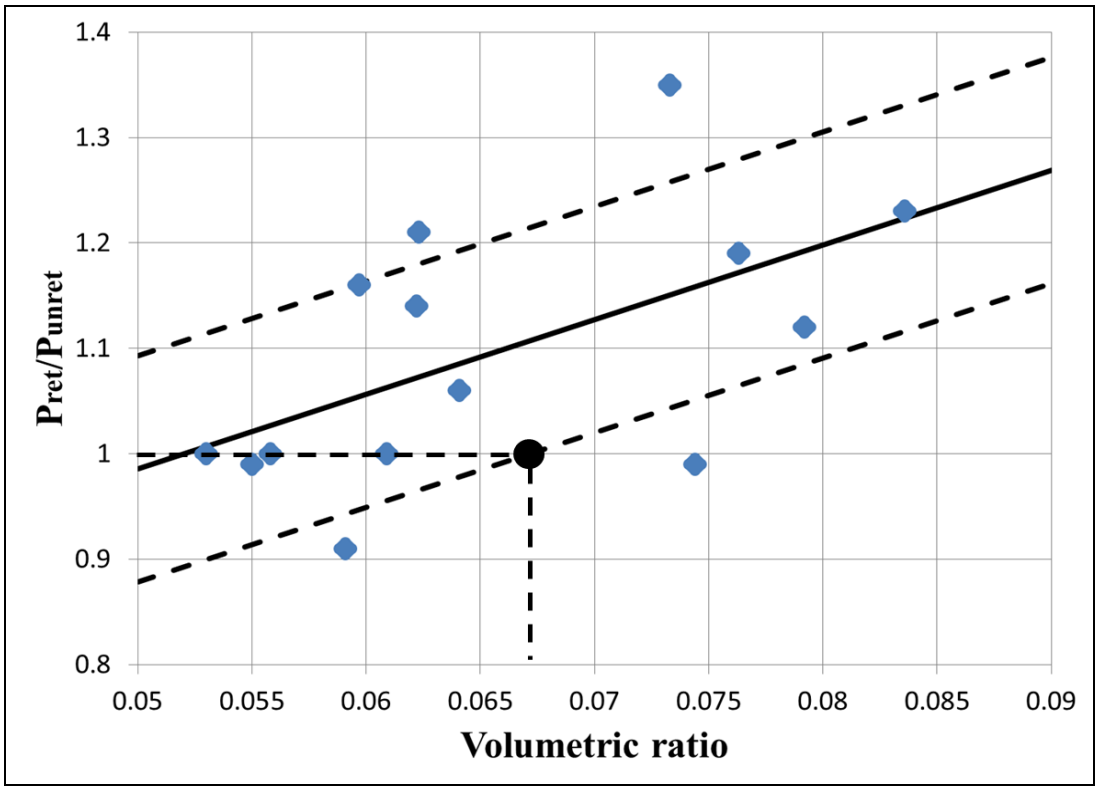

Figure 5-4. Regression analysis of the FRP volumetric ratio vs. ρ_{ret}/ρ_{unret} data points.

It is important to recall that the calculated volumetric ratio corresponds to the GFRP type used in this study. However, it can be generalized to accommodate other FRP types with a different modulus of elasticity, E_{FRP}. The equivalent design FRP volumetric ratio (ρ_{FRP-eq}) can be expressed as follows:

$$\rho_{FRP-eq} = \rho_{FRP}\frac{1800}{E_{FRP}} \tag{5.1}$$

where ρ_{FRP} is the design volumetric ratio of FRP used in this study, with E_{FRP} equal to 1800 ksi (12400 MPa). The number of layers, *n*, of thickness, *t*, needed to retrofit the timber pile post connection can be calculated as:

$$n = \frac{D}{2t}\left(\sqrt{1+\rho_{FRP-eq}}-1\right) \tag{5.2}$$

Finally, Equations 5.1 and 5.2 can be merged to form the following equation:

$$n = \frac{D}{2t}\left(\sqrt{1+\rho_{FRP}\frac{1800}{E_{FRP}}}-1\right) \tag{5.3}$$

As stated above, based on the experimental tests and after a regression analysis, the optimal volumetric ratio ρ_{FRP} is 0.068. Therefore, Equation 5.3 can be simplified to:

$$n = \frac{D}{2t}\left(\sqrt{1+\frac{122}{E_{FRP}}}-1\right) \tag{5.4}$$

where the unit of E_{FRP} is ksi.

CHAPTER 6 CONCLUSIONS

This report focused on (1) presenting an alternative structural load rating method for bridge timber piles that takes into account the effect of interaction of axial force and bending in the pile resulting from the eccentricity of applied vehicular load, and (2) developing a simple and reliable retrofit technique using FRPs to enhance the flexural-compression behavior of "posted" timber piles.

The FE method, along with the modified load rating method, was used to numerically investigate the sensitivity of the critical pile load rating to five geometric and structural bridge parameters: span length, eccentricity of the deck, pile length, skew angle, and deterioration of the piles. The rating obtained from the proposed method was compared with that from the concentric load rating method with the expected geotechnical capacity. The results showed that the proposed method results in more conservative ratings compared to the concentric method in cases with moderate to high levels of pile deterioration.

In the most critical deterioration profile considered in this study (Profile III), the eccentric load rating method governed over the load rating method based on the expected geotechnical capacity for damage levels as low as 30%. The analysis also revealed that, regardless of the type of deterioration in the piles, pile length is the most influential parameter on the load rating of the piles. In three of the four studied damage profiles (undamaged, Profile II, and Profile III), the bridge skew angle had the least impact on the rating of the piles. This study clearly illustrated that considering the effects of eccentric loading in the load rating of bridge timber piles is crucial. This report also presented a simple approach for bridge engineers to use when considering these effects in the load rating of piles.

To evaluate the feasibility of using the FRP retrofit technique to "posted" piles under compression-only loading or flexure-compression loading, a total of twenty pile specimens (four under compression-only and sixteen under compression-flexure) were tested in the study. Each specimen was tested before and after retrofitting with GFRP or CFRP sheets. To assess the impact of realistic field conditions, different details of the FRP retrofit technique were investigated, including applying FRP with and without mortar shell, introducing a mortar-filled wedge in the tested specimen prior to wrapping it with FRP to mimic the effect of severe damage, and "posting" the piles with nails instead of steel drift pins.

Those test results showed acceptable structural behavior for the specimens retrofitted with GFRP sheets, regardless of the retrofit details adopted in the tests. On average, specimens retrofitted with GFRPs showed strength 10% greater than that of unretrofitted specimens. The behavior of CFRP sheets, however, was less satisfactory due to the small thickness of the CFRP shell used as a result of the high strength of CFRP compared to GFRP. This resulted in excessive out-of-plane deformation of CFRP shell under large compressive stress. It was found that using mortar shell along with FRP sheets helps enhance the stiffness of the retrofitted pile; hence, mortar shell is recommended for piles with higher levels of damage. The average mean and median

reduction in stiffness of the retrofitted specimens was 5% and 14% of the unretrofitted specimens, respectively.

Linear regression analysis was conducted on the test data. Using the $\mu \pm 2\sigma$ range, a design value for the FRP volumetric ratio of 6.8% was determined for the GFRP type used in this study. This value was utilized along with the elastic design theory to propose a more generic formula for the design of retrofit for bridge timber piles using any FRP type.

REFERENCES

Ambrose, J., and Tripeny, P. (2009). *Simplified Design of Wood Structures*, 6th ed. New York: John Wiley & Sons.

American Association of State Highway and Transportation Officials (AASHTO) (2002). *Standard Specifications for Highway Bridges*, 17th ed. Washington, DC: AASHTO.

American Association of State Highway and Transportation Officials (AASHTO) (2007). *LRFD Bridge Design Specification*. Washington, DC: AASHTO.

American Forest and Paper Association (AFPA) (2005). *National Design Specification (NDS) for Wood Construction*. Washington, DC: AFPA.

Andrawes, B., and Caiza, P., (2012). "Bridge Timber Piles Load Rating under Eccentric Loading Conditions." *Journal of Bridge Engineering*, 17(4), 700-710.

ANSYS, Inc. (2004). Theory Reference, ANSYS Release 9.0.

Borello, D.J., Andrawes, B., Hajjar, J.F., Olson, S.M., Hansen, J., and Buenker, J. (2009). *Forensic Collapse Investigation of a Concrete Bridge with Timber Piers*. Rep. No. FHWA-ICT-09-042. Rantoul: Illinois Center for Transportation.

Borello, D.J., Andrawes, B., Hajjar, J.F., Olson, S.M., and Hansen, J. (2010). "Experimental and analytical investigation of bridge timber piles under eccentric loads." *Engineering Structures*, 32(8):2237–2246.

Buchanan, A.H. (1986). "Combined bending and axial loading in lumber." *Journal of Structural Engineering*, 112: 2592–2609.

Chellis, R. (1967). *Pile Foundations*, 2nd ed. New York: McGraw Hill, pp. 580–599.

Hagos, M. (2001). *Repair of Heavily Decayed Timber Piles Using Glass Fiber Reinforced Polymers (GFRP) and Cementitious Grout*. M.Sc. Thesis, Department of Civil and Geological Engineering, University of Manitoba, Winnipeg.

Iowa Department of Transportation (Iowa DOT) (2010). *LRFD Bridge Manual Design Commentary C6.2*. http://www.iowadot.gov/bridge/policy/62PileLRFDCJu12.pdf

McCutcheon, W., Gutkowski, R., and Moody, R. (1986). "Performance and rehabilitation of timber bridges." *Transportation Research Record*, 1053:65–79.

Newlin, J.A., and Trayer, G.W. (1956). *Stresses in Wood Members Subjected to Combined Column and Beam Action*. Madison, WI: Forest Products Laboratory.

Steiger, R., and Fontana, M. (2005). "Bending moment and axial force interacting on solid timber beams." *Journal of Materials and Structures*, 38:507–513.

Walpole, R.E., Myers, R.H., Myers, S.L., and Ye, K. (1998). *Probability & Statistics for Engineers & Scientists*, 6th ed. Upper Saddle River, NJ: Prentice Hall.

Wipf, T.J., Fanous, F.S., Klaiber, F.W., and Eapen, A.S. (2003). *Evaluation of Appropriate Maintenance, Repair and Rehabilitation Methods for Iowa Bridges*. Final Report, Iowa DOT Project TR-429.

Wood, L.W. (1950). *Formulas for Columns with Side Loads and Eccentricity*. Madison, WI: Forest Products Laboratory.

Zahn, J.J. (1988). “Combined-load stability criterion for wood beam-columns.” *Journal of Structural Engineering*, 114(11):2612–2628.

APPENDIX A FORCE VS. DISPLACEMENT GRAPHS FOR UNRETROFITTED AND RETROFITTED SPECIMENS

SPECIMEN SP1-C

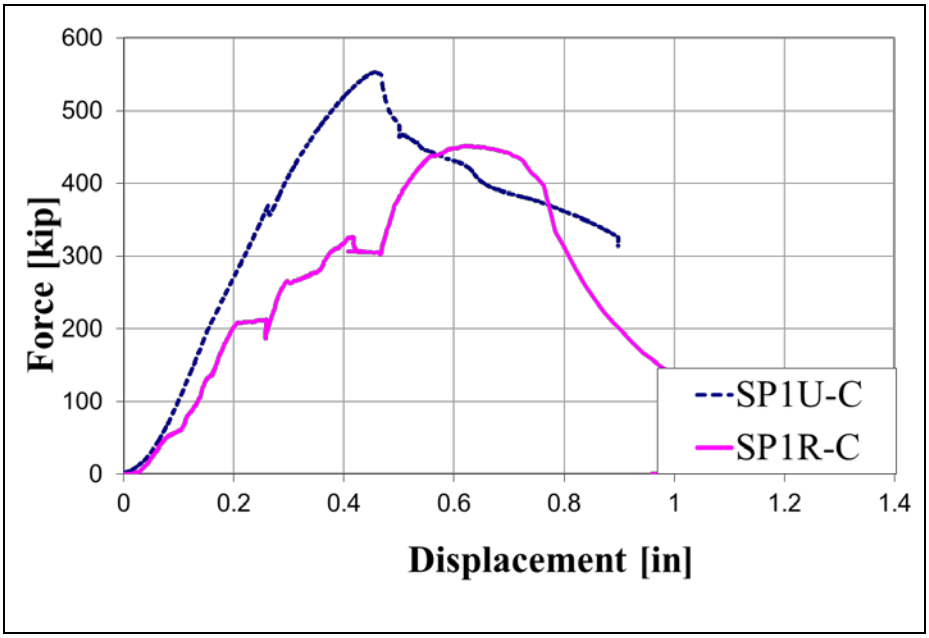

SPECIMEN SP2-C

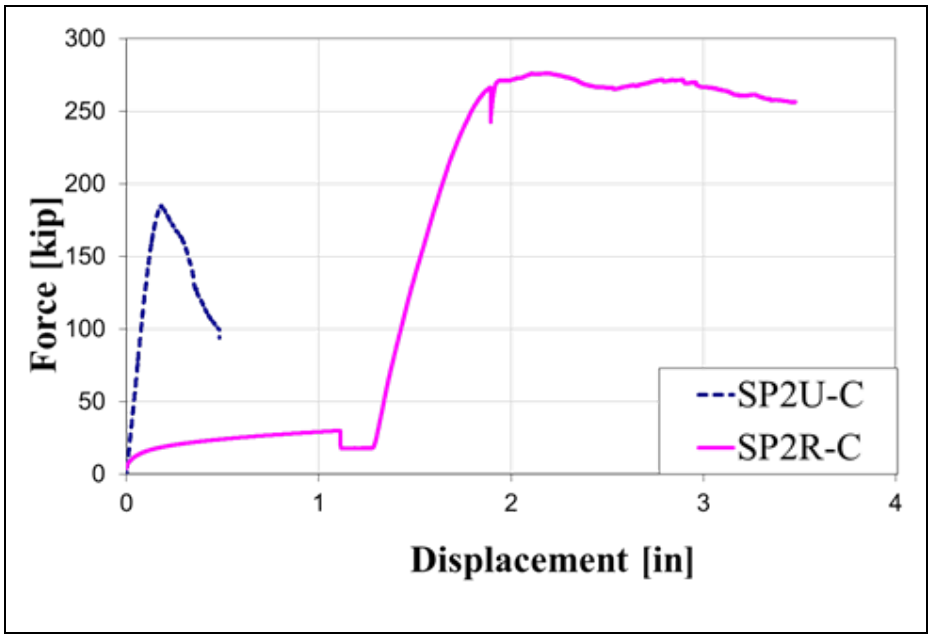

SPECIMEN SP3-C

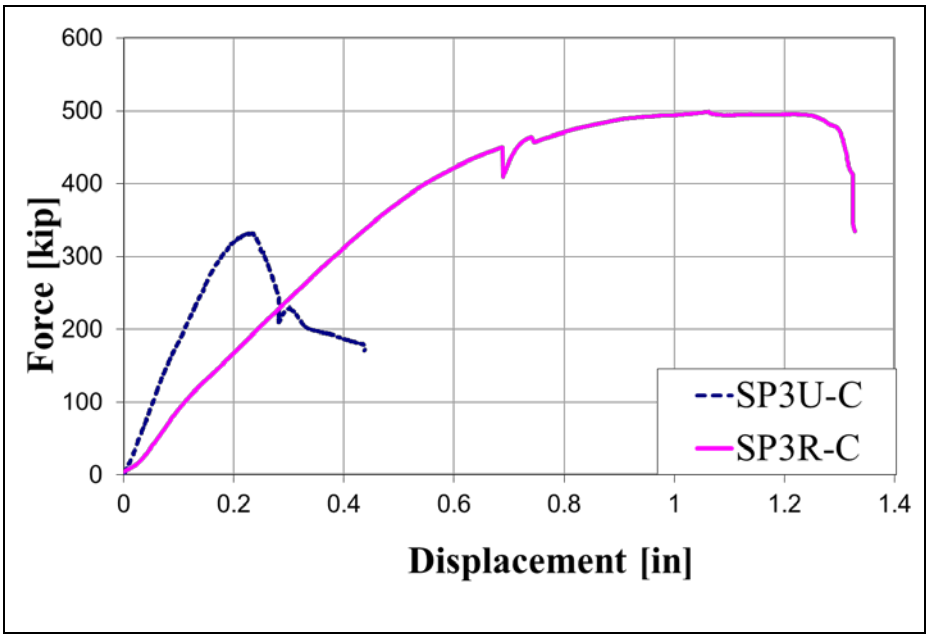

SPECIMEN SP4-C

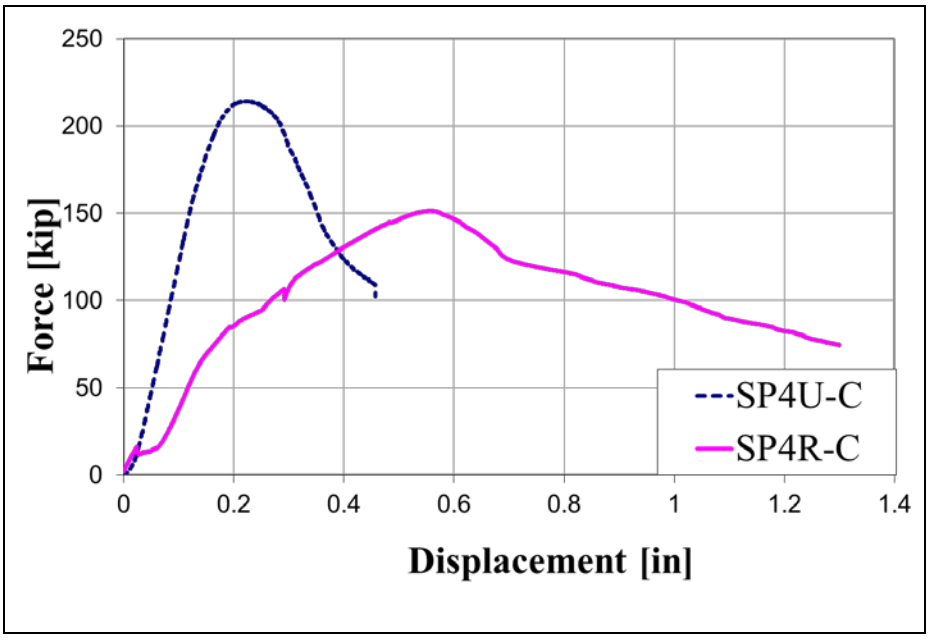

SPECIMEN SP1

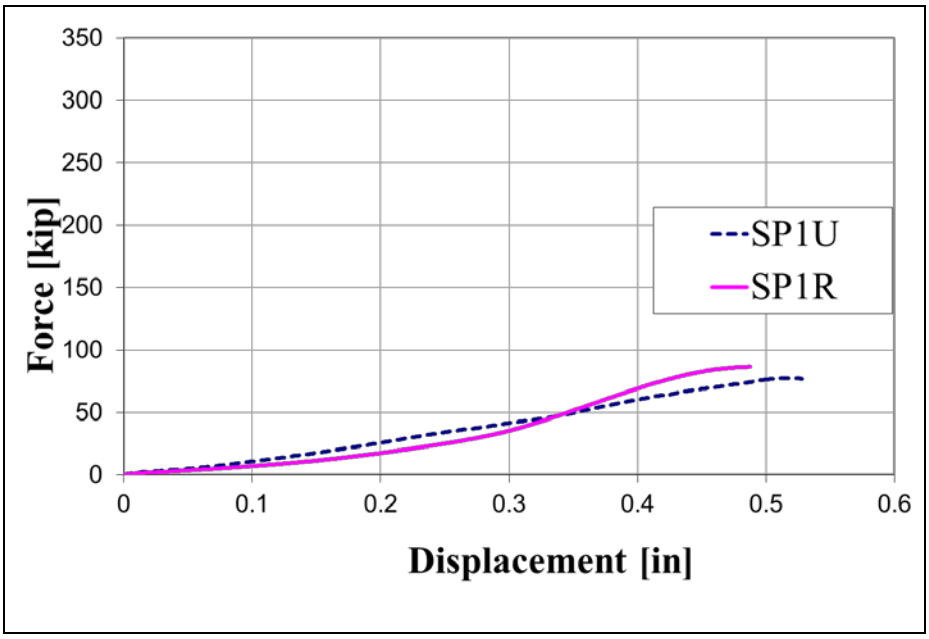

SPECIMEN SP2

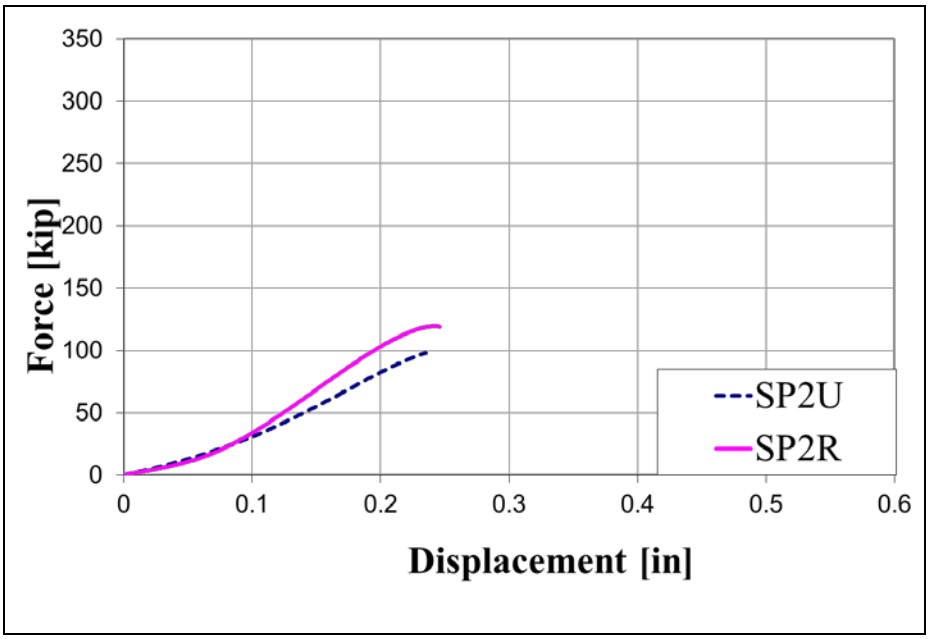

SPECIMEN SP3

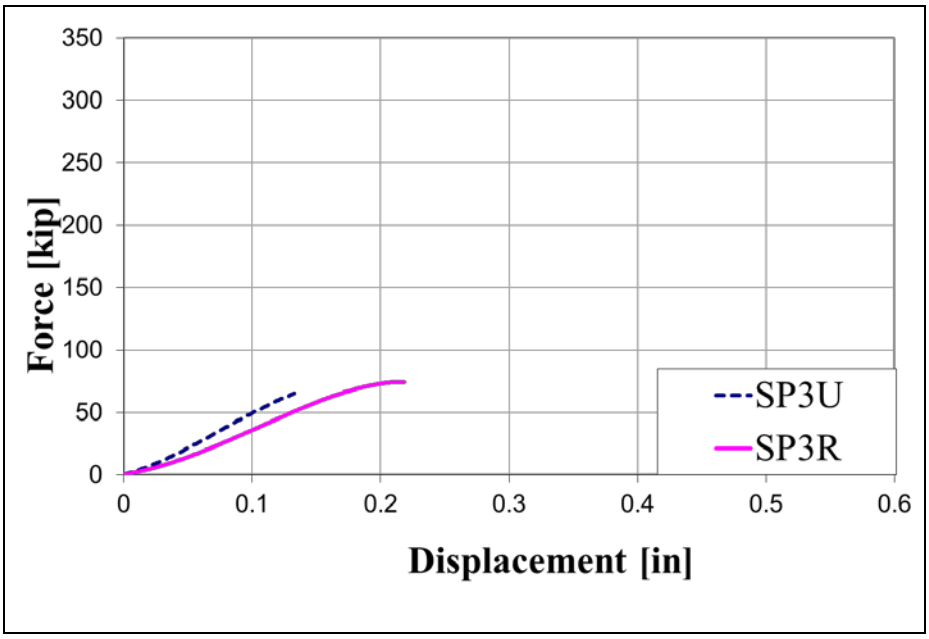

SPECIMENSP4

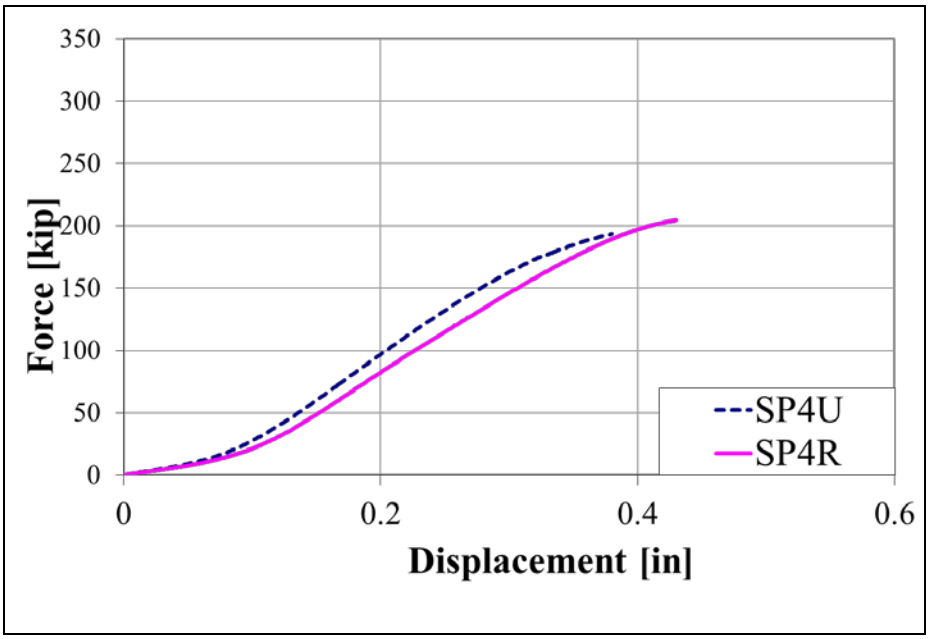

SPECIMEN SP5

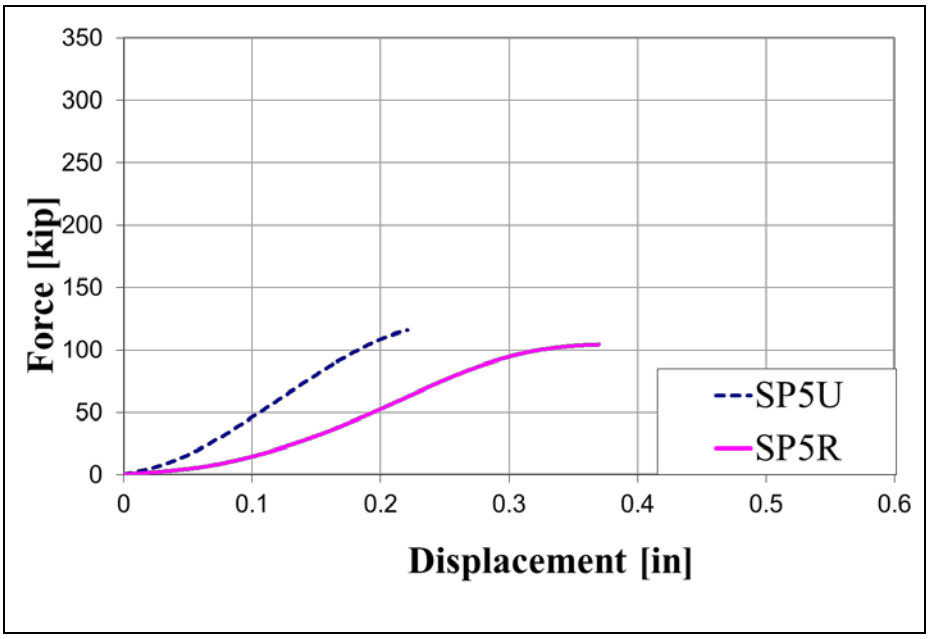

SPECIMEN SP6

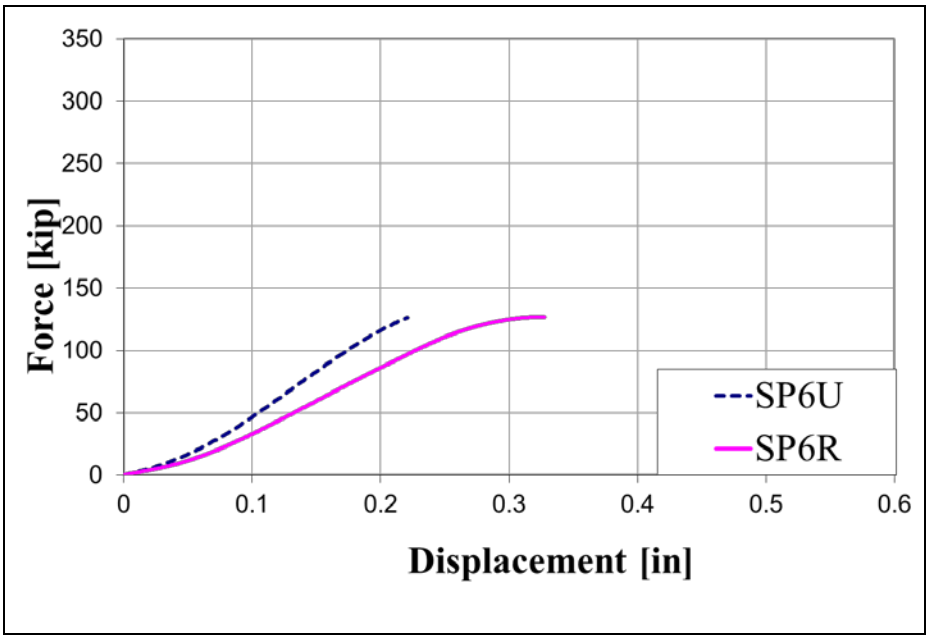

SPECIMEN SP7

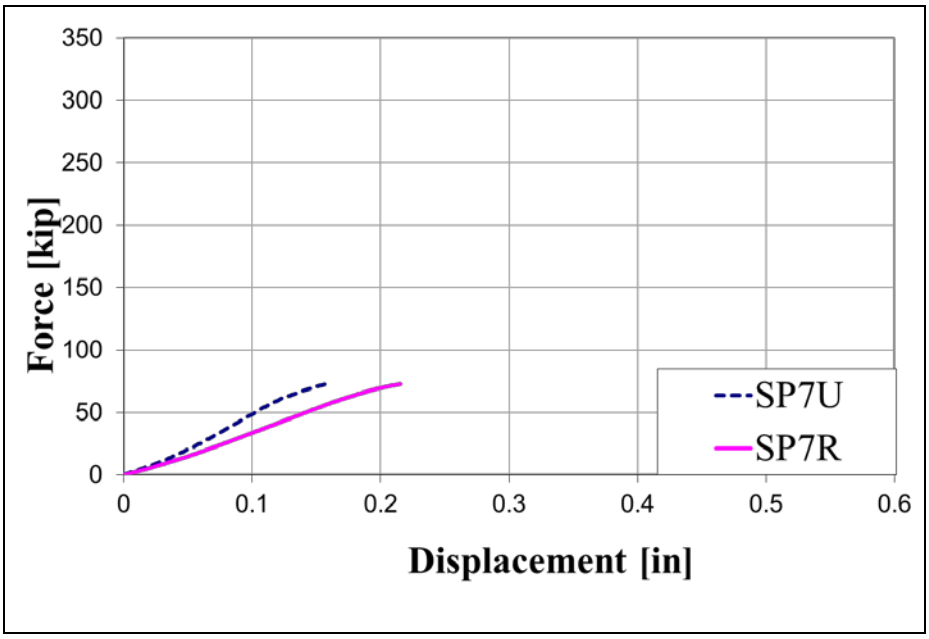

SPECIMEN SP8

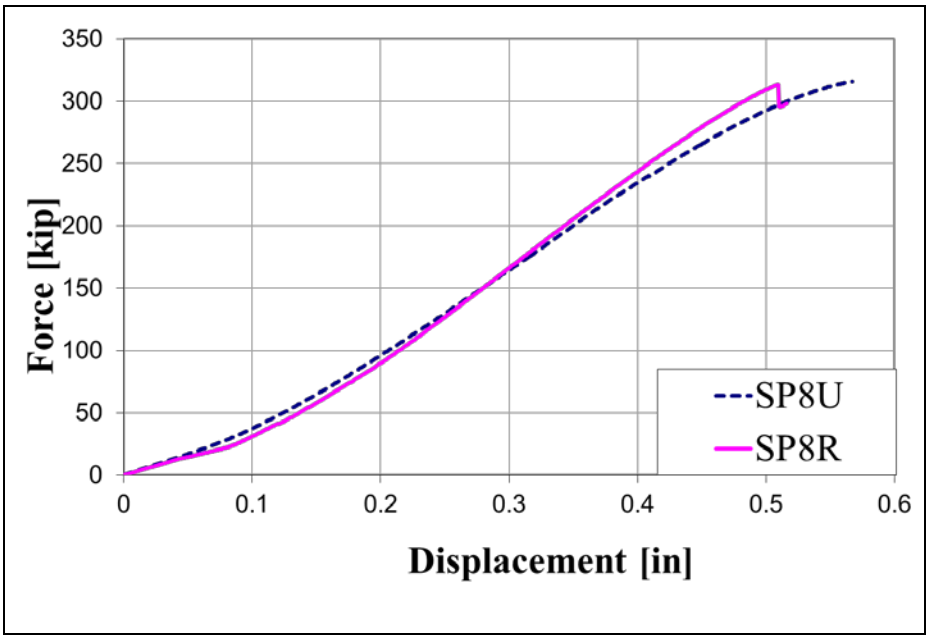

SPECIMEN SP9

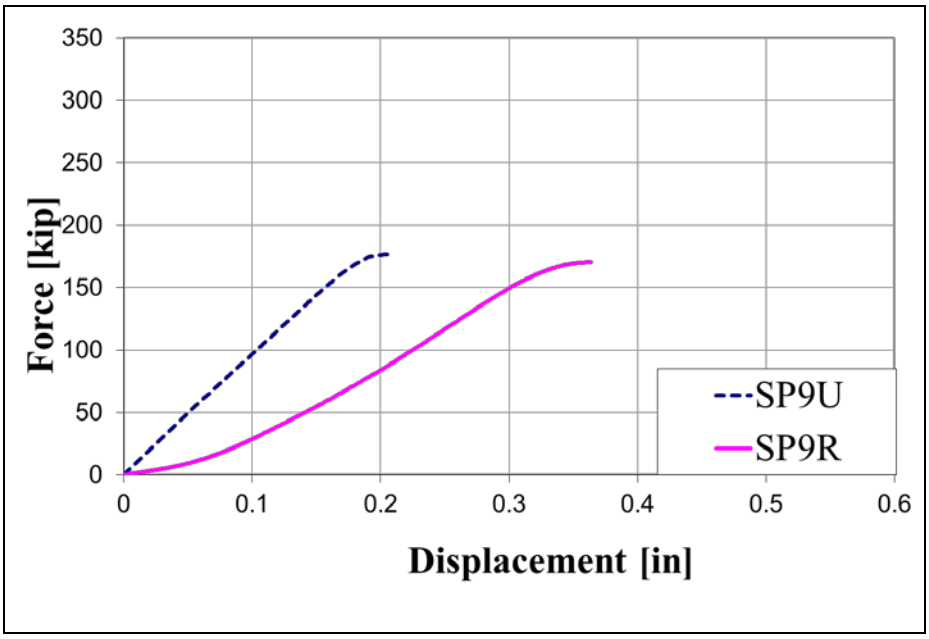

SPECIMEN SP10

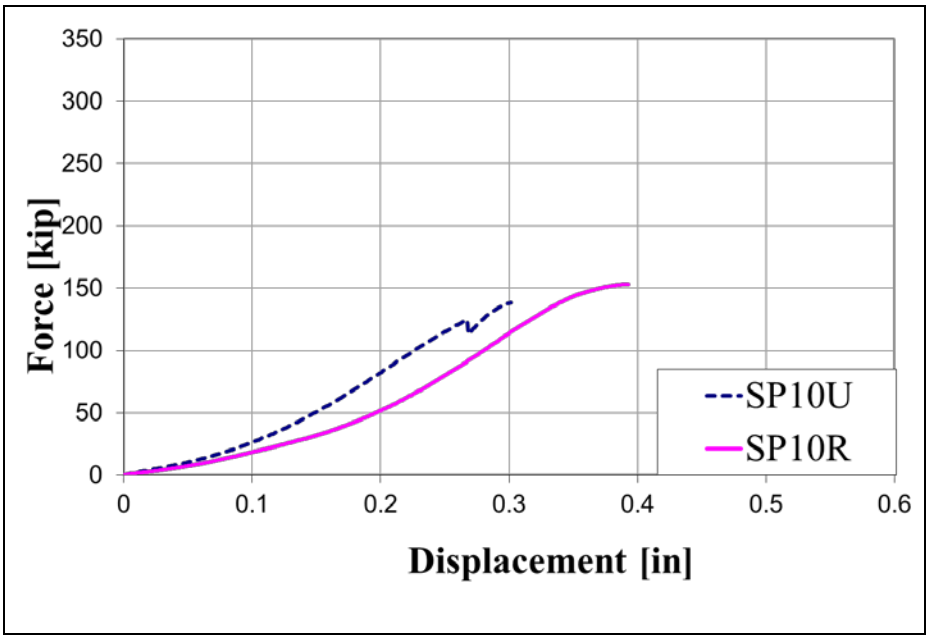

SPECIMEN SP11

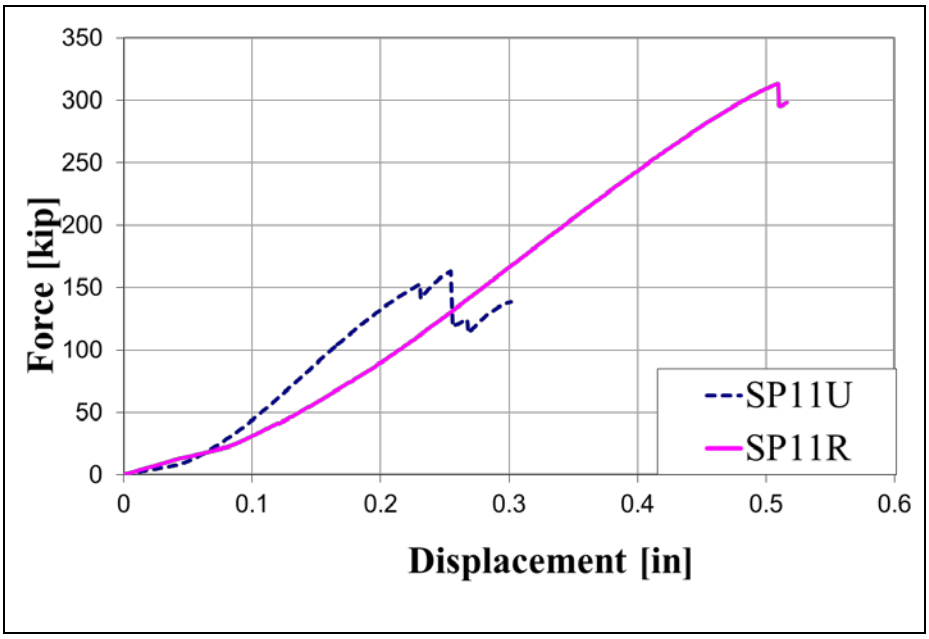

SPECIMEN SP12

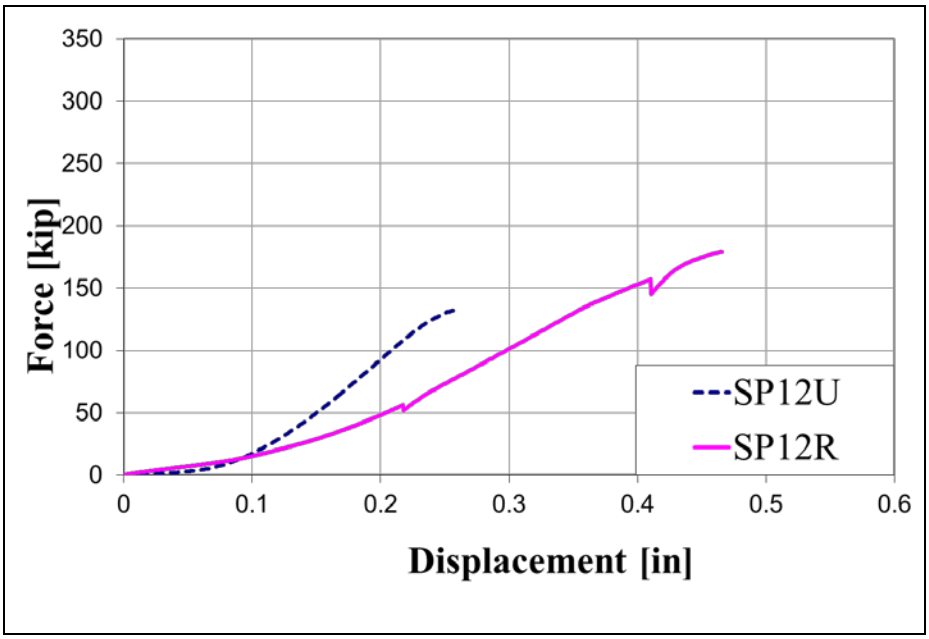

SPECIMEN SP13

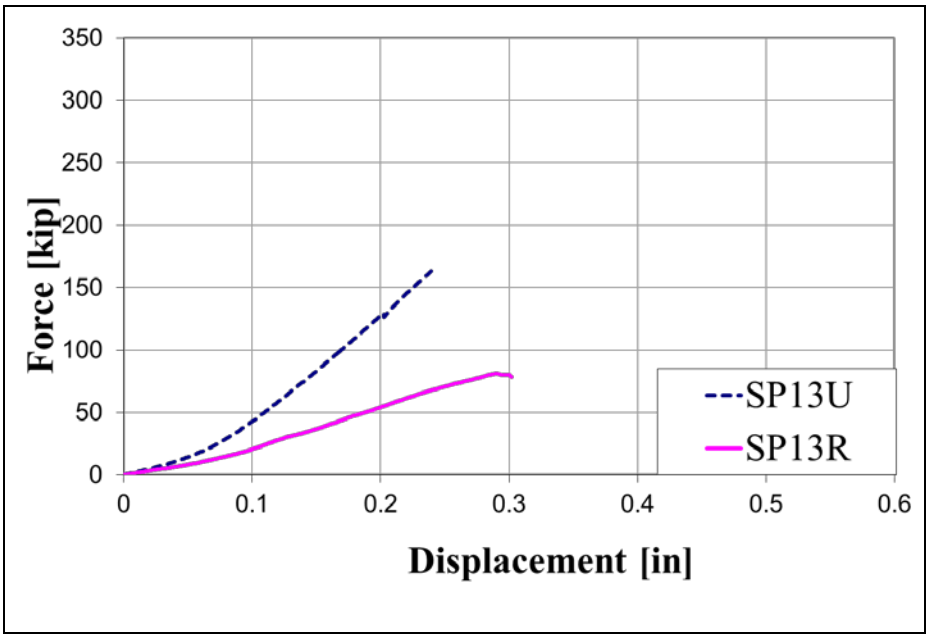

SPECIMEN SP14

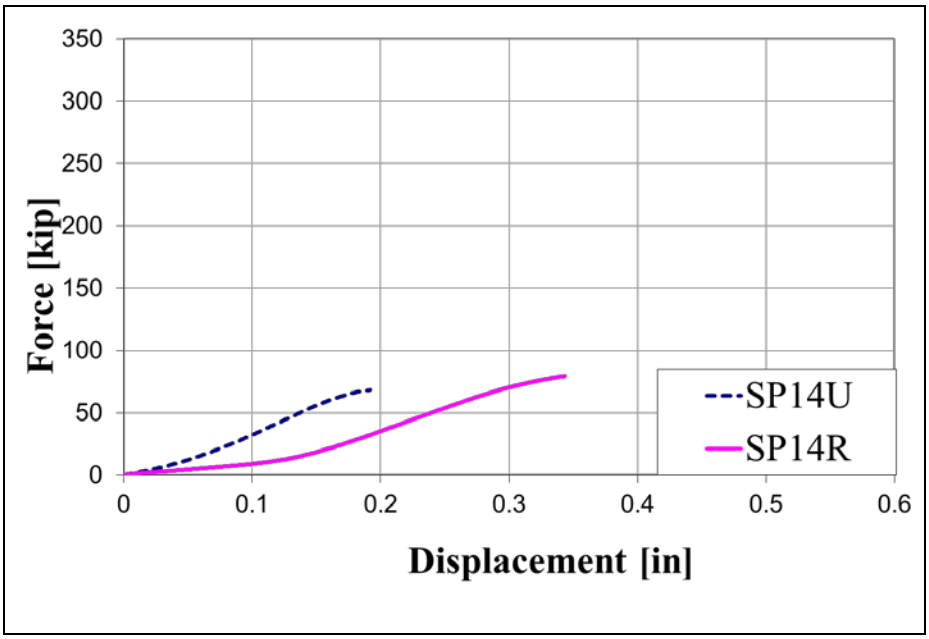

SPECIMEN SP15

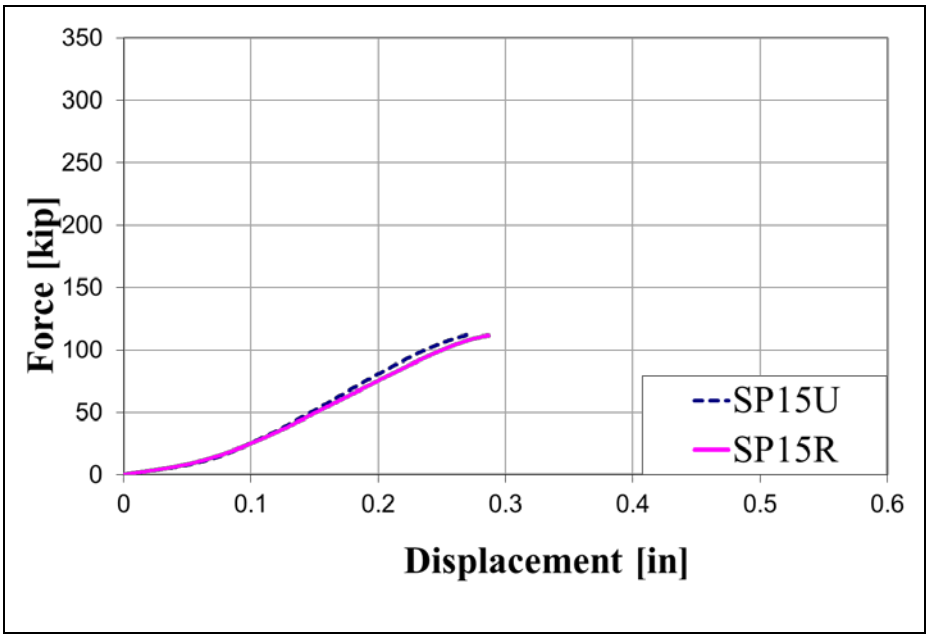

SPECIMEN SP16

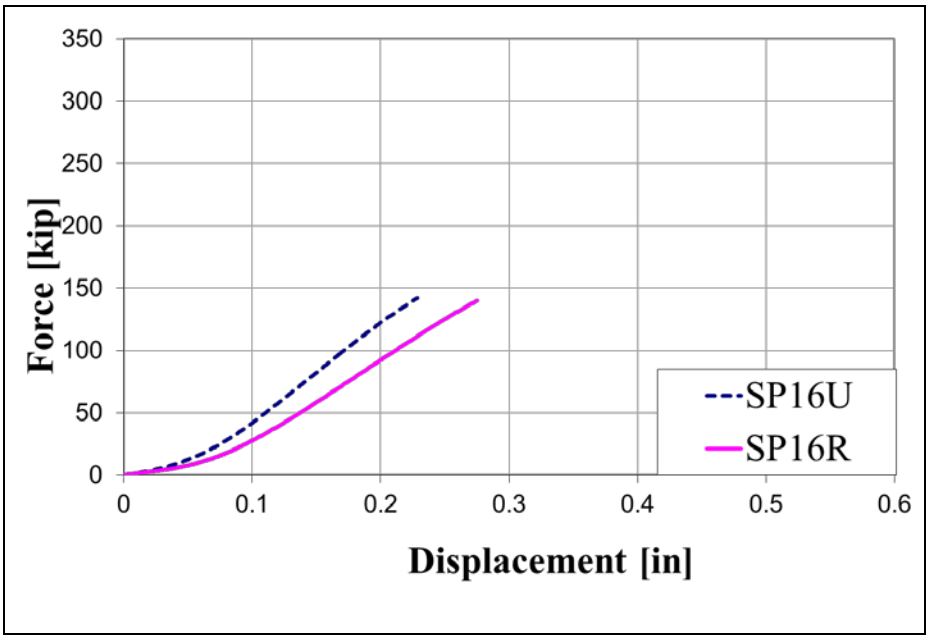


Illinois Department
of Transportation


ILLINOIS
UNIVERSITY OF ILLINOIS AT URBANA-CHAMPAIGN